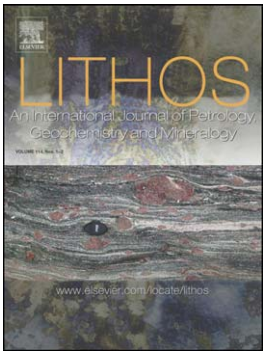

Petrogenesis and tectonic significance of the Late Triassic mafic dikes and felsic volcanic rocks in the East Kunlun Orogenic Belt, Northern Tibet Plateau

Yan Hu, Yaoling Niu, Jiyong Li, Lei Ye, Juanjuan Kong, Shuo Chen, Yu Zhang, Guorui Zhang

PII: S0024-4937(15)00162-0
DOI: doi: 10.1016/j.lithos.2015.05.004
Reference: LITHOS 3590

To appear in: *LITHOS*

Received date: 3 March 2015
Accepted date: 4 May 2015

Please cite this article as: Hu, Yan, Niu, Yaoling, Li, Jiyong, Ye, Lei, Kong, Juanjuan, Chen, Shuo, Zhang, Yu, Zhang, Guorui, Petrogenesis and tectonic significance of the Late Triassic mafic dikes and felsic volcanic rocks in the East Kunlun Orogenic Belt, Northern Tibet Plateau, *LITHOS* (2015), doi: 10.1016/j.lithos.2015.05.004

Petrogenesis and tectonic significance of the Late Triassic mafic dikes and felsic volcanic rocks in the East Kunlun Orogenic Belt, Northern Tibet Plateau

Yan Hu [a, *], Yaoling Niu [a, b, c, *], Jiyong Li [a], Lei Ye [d], Juanjuan Kong [a], Shuo Chen [a], Yu Zhang [d], Guorui Zhang [d]

[a] Institute of Oceanology, Chinese Academy of Sciences, Qingdao 266071, China
[b] Department of Earth Sciences, Durham University, Durham DH11 3LE, UK
[c] School of Earth Science and Resources, China University of Geosciences, Beijing 100083, China
[d] School of Earth Sciences, Lanzhou University, Lanzhou 730000, China

***Corresponding authors:**
Miss Yan Hu (roba.hu@foxmail.com)
Professor Yaoling Niu (yaoling.niu@foxmail.com)

Address: Institute of Oceanology, Chinese Academy of Sciences, No.7 Nanhai Road, Shinan District, Qingdao 266071, China. Tel.: +86 0532 82898980

Abstract

We present zircon U-Pb ages and geochemical data on the late Triassic mafic dikes (diabase) and felsic volcanic rocks (rhyolite and rhyolitic tuff) in the East Kunlun Orogenic Belt (EKOB). These rocks give a small age window of 228-218 Ma. The mafic dikes represent evolved alkaline basaltic melts intruding ~ 8-9 Myrs older and volumetrically more abundant A-type granite batholith. Their rare earth element (REE) and multi-element patterns similar to those of the present-day ocean island basalts (OIB) except for a weak continental crustal signature (i.e., enrichment of Rb and Pb and weak depletion of Nb, Ta and Ti). Their trace element characteristics together with the high $^{87}Sr/^{86}Sr$ (0.7076- 0.7104), low $\varepsilon_{Nd(t)}$ (-2.18 to -3.46), low $\varepsilon_{Hf(t)}$ (-2.85 to -4.59) and variable Pb isotopic ratios are consistent with melts derived from metasomatized subcontinental lithospheric mantle with crustal contamination. The felsic volcanic rocks are characterized by high LREE/HREE (e.g., $[La/Yb]_N$ of 5.71-17.00) with a negative Eu anomaly and strong depletion in Sr and P, resembling the model upper continental crust (UCC). Given the high $^{87}Sr/^{86}Sr$ (0.7213-0.7550) and less negative $\varepsilon_{Nd(t)}$ (-3.83 to -5.09) and $\varepsilon_{Hf(t)}$ (-3.06 to -3.83) than the UCC plus the overlapping isotopes with the mafic dikes and high Nb-Ta rhyolites, the felsic volcanic rocks are best interpreted as resulting from melting-induced mixing with 45-50% crustal materials and 50-55% mantle-derived mafic melts probably parental to the mafic dikes. Such mantle-derived melts underplated and intruded the deep crust as juvenile crustal materials. Partial melting of such juvenile crust produced felsic melts parental to the felsic volcanic rocks in the EKOB. We hypothesize that the late

Triassic mafic dikes and felsic volcanic rocks are associated with post-collisional extension and related orogenic collapse. Such processes are probably significant in causing asthenospheric upwelling, decompression melting, induced melting of the prior metasomatized mantle lithosphere and the existing crust. This work represents our ongoing effort in understanding the origin of the juvenile crust and continental crustal accretion through magmatism in the broad context of orogenesis from seafloor subduction to continental collision and to post-collisional processes.

Keywords**:** alkaline mafic dikes; felsic volcanic rocks; subcontinental lithospheric mantle; crustal anatexis; post collision; East Kunlun Orogenic Belt

1. Introduction

The Late Triassic volcanic rocks are widespread along the East Kunlun Orogenic Belt (EKOB), stratigraphically concentrated in two formations: the Elashan Formation (T_3e) and the Babaoshan Formation (T_3b) (Fig. 1c). The Elashan Formation distributes discontinuously along the entire EKOB with lithologies including abundant basalt, trachyandesite, trachyte, andesite, rhyolite and pyroclastic rocks. Additionally, in its western section there also exist abundant diabasic dikes of alkaline composition (218.1±2.5 Ma) in the volumetrically more abundant A-type granitoids (227.0±3.3 Ma) (Hu et al., in preparation) extending W-E for about 50 kilometers (Fig. 2a, b, c). Significant volumes of coeval felsic volcanic rocks (227.5±1.5 Ma to 219.5±1.9 Ma) crop out toward its eastern section (Fig. 2d, e). Mafic dikes of mantle

origin provide key information on their petrogenesis in particular and geodynamic processes in general. They can be derived from asthenospheric mantle associated with subduction, rift and mantle plume activities (Buchan et al., 1998; Chen et al., 2011; Goldberg, 2010; Hoek and Seitz, 1995; Srivastava, 2011; Stepanova and Stepanov, 2010), but they can also result from melting of subcontinental lithospheric mantle (SCLM) in response to surface extension and lithosphere thinning (Liu et al., 2012; Williams et al., 2001). The origin of felsic volcanic rocks coeval with the alkaline mafic rocks is commonly interpreted as resulting from (1) advanced extent of fractional crystallization of mantle-derived mafic magmas directly (Shao et al., 2015; Tian et al., 2010; Turner et al., 1992), (2) partial melting of crust triggered by heating of mantle-derived mafic magmas (Christiansen et al., 1983; Huppert and Sparks, 1988; Ratajeski et al., 2001; Takanashi et al., 2011), and (3) hybridization of crustal melts with mantle-derived mafic melts (Ding et al., 2011; Yang et al., 2008).

The EKOB is one of the major tectono-magmatic belts on the Greater Tibetan Plateau. It records a long history of magmatism and tectonic evolution beginning in the Early Paleozoic and continuing into the Cenozoic (Ding et al., 2011; Mo et al., 2007; Xiong et al., 2013; Yang et al., 1996). The paleo-ocean recorded by the EKOB between Laurasia and Gondwana has been regarded as having undergone multi-cycle tectonic evolution with opening and closing of Pre-Prototethys, Prototethys and Paleotethys oceans (Yin and Zhang, 1997). The latest opening-closing cycle recorded by the EKOB is termed the A'nyemaqen Ocean (Jiang et al., 1992; Mo et al., 2007), which is thought to be the north branch of the Paleotethys Ocean (Jiang et al., 1992;

Yang et al., 1996). The timing of the A'nyemaqen seafloor subducting, closing and continental collision remains controversial. Many consider that the seafloor subduction occurred during the Late Permian to Middle Triassic (Harris et al., 1988) with continental collision in the Late Triassic (Guo et al., 1998; Liu et al., 1984; Luo et al., 2002; Mo et al., 2007), but others differ. For example, Pan et al. (2012) proposed that the EKOB records a syn-collisional setting in the Early to Middle Triassic and a post-collisional setting in the Late Triassic. Yang et al. (2009) argued that the A'nyemaqen Ocean opened as early as the Late Carboniferous (308Ma) and was closed probably during the Early Triassic, as marked by island arc volcanic rocks of the Late Permian age (260Ma), back arc basin basalts in the Early-Middle Triassic and the post-collisional volcanic rocks in the Late Triassic. Recently, Xia et al. (2014) proposed, using new data and data in the literatures, that seafloor subduction started at ~ 260Ma (Late Permian), lasting for 20Myrs before continental collision from 240 to 232Ma (Middle Triassic).

Previous studies have been focused on the volcanic rocks from the eastern section of the EKOB (Ding et al., 2011; Li et al., 2013a; Liu et al., 2014a; Xiong et al., 2014a; Yang et al., 2009; Zhu et al., 2006). In this paper, we report the coeval mafic dikes together with rhyolitic volcanic rocks along the entire EKOB. More importantly, to reveal the petrogenesis of the late Triassic mafic dikes and felsic volcanic rocks and the regional tectonic setting of the EKOB in the Late Triassic, we present new high-quality zircon U-Pb ages for both mafic dikes and felsic volcanic rocks from each section of the EKOB and their bulk-rock major element, trace element and

Sr-Nd-Pb-Hf isotopic compositions. Using these data, we discuss the petrogenesis of these sub-volcanic and volcanic rocks in the context of the EKOB evolution.

2. Geological setting and samples

The Tibetan Plateau is a huge composite terrane amalgamated through multiple continental collision events expressed by progressively younger sutures from northeast in the early Paleozoic to southwest in the Cenozoic (Harris et al., 1988; Niu et al., 2013). The East Kunlun-Qaidam terrane is constrained between the south Qilian suture and Anyemaqen-Kunlun-Mutztagh suture, south of which is referred to as the Kunlun batholith dominated by a broad Early Paleozoic arc and a narrower Late Permian to Traissic arc (Yin and Harrison, 2000) (Fig. 1a). The EKOB is bounded by the Qaidam Basin to the north and Hoh Xil-Songpan-Ganze Basin to the south, which can be divided into three zones: northern (Qimantagh folded zone), middle (granite zone) and southern zones by major faults (i.e., South Kunlun Fault and Central Kunlun Fault) (Fig. 1b; Jiang et al., 1992). Particularly, the northern and middle zones show abundant magmatism (Fig. 1b and c; Yuan et al., 2000).

The continental crust basement of the main magmatism zone of the EKOB is represented by the Paleo- and Mesoproterozoic Jinshuikou Group comprising the lower Baishahe and upper Xiaomiao formations. The lower Baishahe Formation consists of marbles, gneisses, migmatites and amphibolites. The upper Xiaomiao Formation comprises marbles, gneisses, greenschists and quartzites (Jiang et al., 1992; Liu et al., 2014a; Mo et al., 2007; Ren et al., 2010; Xiong et al., 2014a). The EKOB is

characterized by abundant magmatism manifested by the widespread intrusive and volcanic rocks, especially the granitoids and some ophiolitic remnants representing long-lasing magmatic activities from the Proterozoic to the late Mesozoic, which are principally distributed north of the Central Kunlun Fault (Fig. 1; Mo et al., 2007).

The late Triassic mafic dikes and felsic volcanic rocks in the EKOB are all fresh and representative samples collected from the Elashan Formation, including diabases, rhyolitic tuffs and rhyolite porphyries. The mafic dikes intruding the ~ 8-9 Myrs older A-type granite batholith (see below) are best exposed and sampled in the Yeniugou area ("YNG" in Fig. 1c; Fig. 2a; Table 1). The dikes are mostly aphyric (< 5% crystals) with minor plagioclase phenocrysts. The groundmass, with a holycrystalline/diabasic texture, is made up of quench microlites of plagioclase, pyroxene, olivine and opaques (Fig. 2c). The rhyolitic tuffs mainly crop out in the Tufangzi area ("QMX" in Fig. 1c; Table 1), containing glass shards (~60%), crystal clasts of quartz (with melt corrosion/absorption features), plagioclase and biotite (~25% in total) and rhyolite fragments (~15%) (Fig. 2d). The rhyolite porphyry is well exposed and sampled in the Reshui and Yingde'er areas closing to Dulan County ("RSX" and "YDE" in Fig. 1c; Table 1). The phenocrysts are mostly quartz (with melt corrosion shapes), and minor feldspar and biotite (~15% in total) in the glassy groundmass (Fig. 2e).

3. Sample preparation and analytical methods

Twenty-seven fresh samples were analyzed for major and trace elements and eleven of them were selected for Sr, Nd, Pb and Hf isotopic analyses (Pb isotopes

done only for the mafic dikes). Three representative samples were chosen for zircon U-Pb dating.

3.1. Zircon U-Pb dating

Zircon crystals were selected using techniques of heavy liquid and magnetic separation, followed by hand-picking before mounted in epoxy resin and polished down to ~ half thickness (Song et al., 2002; Xiu et al., 2001). Cathodoluminescence (CL) images were obtained using a CL spectrometer (Gatan MonoCL4+) equipped on a FEI Quanta 450 FEG scanning electron microscope (SEM) at China University of Geosciences, Wuhan (CUGW) to reveal their internal structures and to choose spots for U-Pb analysis. The working condition is 0.8-1Kv for Gatan MonoCL4+ and 10Kv for SEM.

Zircon U-Pb dating and trace element analysis were completed synchronously using laser ablation inductively coupled plasma mass spectrometry (LA-ICP-MS) at CUGW. Detailed operation conditions for laser ablation and ICP-MS analyses are given in Liu et al. (2010a). The spot diameter is 32 μm. Data were processed using ICPMSDataCal (Liu et al., 2010a; Liu et al., 2010b). Concordia diagrams and weighted mean calculations were done using Isoplot/Ex_version 3.0 (Ludwig, 2003).

3.2. Geochemistry

Pen and saw marks on all samples were removed in the clean laboratory of the Langfang Institute of Regional Geology and Mineral Investigation, China. Samples

that had obvious phenocrysts were reduced to 0.5-2mm size chips for hand picking under a binocular microscope to select "melt" compositions (i.e., class shards and fine-grained aphyric portions of the ground mass) followed by ultrasonic cleaning in Milli-Q water, drying and grinding in agate mortars. Aphyric samples with no phenocrysts were reduced to 5-8mm size chips, cleaned and ground similarly in an agate mill. All the sample powders were ensured to have grain size smaller than 200 mesh under thoroughly clean conditions at Lanzhou University.

3.2.1. Major and trace elements

Major element analysis was done using a Leeman Prodigy inductively coupled plasma-optical emission spectroscopy (ICP-OES) system with high dispersion Echelle optics at China University of Geosciences, Beijing (CUGB). About 35 mg powder of each sample was thoroughly dissolved in the mixture of equal HNO_3 and HF in a Teflon bomb, diluted into 5% HNO_3 solution, and analyzed using an Agilent-7500a inductively coupled plasma mass spectrometry (ICP-MS) at CUGB for trace elements. Sample digestion and analytical details are given by Song et al. (2010).

3.2.2. Sr-Nd-Pb-Hf isotopes

Samples YNG12-03, YNG12-05, QMX12-01, QMX12-08, QMX12-11, RSX12-48 and YDE12-02 were chosen for whole-rock Sr-Nd-Hf isotopic analysis at CUGW. Hf isotopic analysis for samples DL09-01 and DL09-03 (from Ding et al., 2011) was also done at CUGW. About 100 mg rock powder was digested in the

mixture of HNO_3+HF in Teflon bombs in a clean oven at about 190°C for a week. The chemical separation was done following the procedure by Yang et al. (2010). The Sr, Nd isotopic analysis was done on a Thermo Finnigan Triton Ti Thermal Ionization Mass Spectrometer (TIMS), and Hf isotopic analysis was done using a Thermo Neptune Plus Multi-Collector Inductively Coupled Plasma Mass Spectrometer (MC-ICP-MS). The Pb isotopic analysis for samples YNG12-03, YNG12-05, YNG12-01 and YNG12-08 was done in the Radiogenic Isotope Facility at The University of Queensland (UQ), Australia (see below).

For samples YNG12-01 and YNG12-08, the whole-rock Sr, Nd, Pb and Hf isotopic analysis was done at UQ. About 200 mg sample powder was digested in the mixture of double-distilled concentrate HNO_3 and HF, and dried down on a hot plate at 80 °C. After converting any fluoride to nitrate, the dried residue was dissolved with 3ml 2N HNO_3. 1.5ml was loaded onto a stack of Sr-spec, TRU-spec, and Ln-spec resin columns to separate Sr, Pb and Nd from matrix using a modified procedure following Deniel and Pin (2001), Míková and Denková (2007) and Pin and Zalduegui (1997) (also see Guo et al., 2014); another 1.5ml was used to pass through a Ln-spec resin column for Hf separation following Yang et al. (2010). The Sr, Nd, Pb and Hf isotopic ratios were measured on a Nu Plasma HR MC-ICP-MS.

4. Analytical data

4.1. Zircon U-Pb ages

Representative CL images of analyzed zircons and corresponding concordia

diagrams are shown in Fig. 3 and Fig. 4 respectively. The age data are given in Table 2. Zircons from the mafic dikes are pale green and those from the felsic volcanic rocks are pale brown and dark red. They yield weighted mean $^{206}Pb/^{238}U$ ages ranging from 228 to 218 Ma, similar to the age of the A-type granite (see below), which suggests that they are coeval within analytical error (Fig. 4), although the mafic dikes with chilled margins (Fig. 2b) are ~ 8-9 Myrs younger than the host A-type granites (see below).

Zircons from dike sample YNG12-03 are euhedral columnar crystals (80-150 μm long) with aspect ratios of ~ 1.5:1-2:1 (some fragments could be fractured/produced during separation, Corfu et al., 2003) (Fig. 3a). In CL images, they show lower homogeneous luminescence and less obvious regular oscillatory zoning than those in rhyolitic rocks (Fig. 3). The LA-ICP-MS U-Pb analysis gives variable Th (242-2508 ppm) and U (658-7565 ppm) concentrations with Th/U ratios of 0.25-0.67 (Table 2), which are consistent with their being of magmatic origin (Belousova et al., 2002; Hoskin and Schaltegger, 2003). Thus the youngest U-Pb age group of the zircons is probably the crystallization age of the rock. Twelve zircons from this sample plot in-group on the concordia and yield a weighted mean $^{206}Pb/^{238}U$ age of 218.1±2.5 Ma (MSWD =2.9) (Fig. 4a). This age is taken to represent the extrusive age of the mafic dikes. Zircons from the host A-type granite yield a weighted mean $^{206}Pb/^{238}U$ age of 227.0±3.3 Ma (MSWD =3.4) (Hu et al., in preparation), i.e., the host A-type granite emplaced ~ 8-9 Myrs prior to the dike intrusion, probably different products of a generally the same thermal event.

Zircons from rhyolitic tuff sample QMX12-01 are dark red, euhedral columnar crystals (80-250 μm long) with aspect ratios of ~ 1:1-3:1. Their CL images display high homogeneous luminescence and strong oscillatory zoning (Fig. 3b). They have varying Th (185-580 ppm) and U (406-1040 ppm) concentrations with Th/U ratios of 0.44-0.66, consistent with the zircons being of magmatic origin (Table 2; Belousova et al., 2002; Hoskin and Schaltegger, 2003). Twenty-two zircons form a tight cluster with a weighted mean $^{206}Pb/^{238}U$ age of 219.5±1.9 Ma (MSWD =2.5) (Fig. 4b), which is considered as approximating the extrusive age of the rhyolitic tuff representing the felsic volcanism of the EKOB (Note: zircons crystallized in magma chambers prior to eruption).

Rhyolite porphyry sample RSX12-48 was collected from the Reshui area in the east section of the EKOB southeast to Dulan County (Fig. 1). Zircons from this sample are dark red and euhedral columnar crystals (90-250 μm long) with aspect ratios of ~ 1:1-3.5:1 except for some presenting imperfect crystals in CL images. They have lower luminescence (compared with QMX12-01) and obvious oscillatory zoning (Fig. 3c). Zircons from RSX12-48 have variable Th (214-3615 ppm) and U (275-7463 ppm) contents with Th/U ratios of 0.34-0.81 which confirm their magmatic origin (Table 2; Belousova et al., 2002; Hoskin and Schaltegger, 2003). Twelve analyses form a cluster close to the concordia with a weighted mean $^{206}Pb/^{238}U$ age of 227.5± 1.5 Ma (MSWD =0.48) (Fig. 4c). We interpret this as approximating the extrusive age of the rhyolite porphyry from the EKOB.

4.2 Major elements

Whole-rock major and trace element analyses are given in Table 3. The late Triassic mafic dikes and felsic volcanic rocks from the EKOB plot in the fields of basaltic trachyandesite, basaltic andesite, trachyte, trachyte-rhyolite and rhyolite on the total alkali-silica (TAS) diagram (Fig. 5a; Le Bas et al., 1986). In addition, the mafic rocks mainly plot in the alkaline field whereas the felsic volcanic rocks mostly plot in subalkaline division (Irvine and Baragar, 1971).

The mafic rocks represent variably evolved melts characterized by moderate silica (50.35-56.44 wt.%), high Al_2O_3 (16.64-17.76 wt.%) and low $Mg^{\#}$ (0.47-0.54) ($Mg^{\#}$ = molar Mg/[Mg+Fe^{2+}]). They have varying alkaline (Na_2O+K_2O) contents (3.68-7.11 wt.%) and plot in high-K calc-alkaline and shoshonite fields (K_2O = 1.22-2.69 wt.%) (Fig. 5b; Rickwood, 1989). The felsic volcanic rocks have higher silica (66.23-76.02 wt.%) and alkaline (Na_2O+K_2O) (6.70-9.35 wt.%), lower MgO (0.11-1.24 wt.%) and Al_2O_3 (12.81-15.95 wt.%) as expected. They are mainly in the high-K calc-alkaline series with two samples belonging to calc-alkaline series and three in shoshonite series (K_2O = 2.74-5.70 wt.%) (Fig. 5b; Rickwood, 1989). In SiO_2 variation diagrams, major element oxides show expected first-order trends except for Na_2O, although they are unlikely related by liquid lines of descent (LLDs) given the differences of these samples in time and space (Fig. 6).

4.3 Trace elements

In the chondrite normalized rare earth element (REE) diagram, the mafic rocks

are enriched in light REEs with very high $(La/Yb)_N$ (13.22-17.41) and a weak negative Eu anomaly (Eu/Eu^* = 0.81-0.97) (Table 3; Fig. 7a). In primitive mantle normalized multi-element diagram (Fig. 7b), they display moderate enrichment in Rb and Pb and weak depletion in Nb, Ta and Ti.

Felsic volcanic rocks show enrichment in LREEs relative to HREEs with $(La/Yb)_N$ of 5.71-17.00. In the chondrite normalized REE pattern diagram, they show significant negative Eu anomalies (Eu/Eu^*=0.12-0.73) (Table 3; Fig. 7c). Compared with the upper continental crust, the felsic rocks are strongly depleted in Sr and P (Fig. 7d). The large Eu and Sr depletion is consistent with significant plagioclase crystallization as shown petrographically (see Niu and O'Hara, 2009; Fig. 2) during magma evolution from their respective parental melts although varying extent of crustal melting with plagioclase present as a residual phase can also give similar patterns.

4.4 Whole rock Sr-Nd-Pb-Hf isotopes

The isotopic analyses are given in Table 4-6. The initial isotopic ratios are calculated using zircon U-Pb ages of representative samples of this study (see above).

The mafic dikes have present-day $^{87}Sr/^{86}Sr$ of 0.7076-0.7104 (Initial $^{87}Sr/^{86}Sr$ [I_{Sr}] = 0.7070 to 0.7086), giving a positive correlation with SiO_2 (Fig. 8c). They display slightly enriched Nd and Hf isotopic compositions ($\varepsilon_{Nd(t)}$ = -2.18 to -3.46, $\varepsilon_{Hf(t)}$ = -2.85 to -4.59), showing an inverse trend between $\varepsilon_{Nd(t)}$ and SiO_2 (Fig. 8d). The $^{206}Pb/^{204}Pb$, $^{207}Pb/^{204}Pb$ and $^{208}Pb/^{204}Pb$ ratios of the mafic dikes are 18.789-18.850, 15.644-15.651

and 38.777-38.841, respectively, which may suggest an enriched mantle source of the mafic dikes (see below).

The felsic volcanic rocks have overlapping Nd and Hf isotopes with the mafic dikes ($\varepsilon_{Nd(t)}$ = -3.83 to -5.09 and $\varepsilon_{Hf(t)}$ = -3.06 to -3.83) (also see Fig. 9b). However, the present-day $^{87}Sr/^{86}Sr$ ratios of the felsic rocks are variably high (0.7213 to 0.7550) with I_{Sr} = 0.7083-0.7097 (Figs. 8c, 9d) because of the very high Rb/Sr ratios and the strong Sr depletion (see Fig. 7; Table 4).

5. Discussion

5.1. Petrogenesis of the mafic dikes

5.1.1 Crustal contamination

The mafic dikes have evolved alkaline basaltic composition (Fig. 5). Their trace element systematics are indicative of crustal contamination with elevated abundances of Rb, U and Pb and depletion in Nb, Ta and Ti (Fig. 7; Niu and O'Hara, 2009; Rudnick and Gao, 2003). Also, upper continental crust is characterized by high $^{87}Sr/^{86}Sr$ and low $^{143}Nd/^{144}Nd$ ratios (Liu et al., 2004). Therefore, continental crust derived melts are expected to have lower Nb/Th, Ta/U, $\varepsilon_{Nd(t)}$ and higher $^{87}Sr/^{86}Sr$ than mantle-derived melts (Fig. 8; Goldstein and Jacobsen, 1988; Rudnick and Gao, 2003). Given the relative incompatibility of $D_{Nb} \approx D_{Th} < D_{Ta} \approx D_U$ during basaltic magmatism (Niu and Batiza, 1997; Niu and O'Hara, 2009), Nb/Th and Ta/U ratios will remain constant during magmatism and their variation, if any, in samples would be inherited from the source rocks or source histories. If such mafic magmas were

contaminated by the crust, the Nb/Th, Ta/U and $\varepsilon_{Nd(t)}$ would decrease whereas $^{87}Sr/^{86}Sr$ would increase with increasing SiO_2. Indeed, the mafic dikes show inverse correlations of Nb/Th, Ta/U and $\varepsilon_{Nd(t)}$ with SiO_2 (Fig. 8a, b and d), and a positive correlation of $^{87}Sr/^{86}Sr$ with SiO_2 (Fig. 8c). This is also clear in Ta*-Nb* space (Fig. 10), with Nb* < 1 and Ta* < 1, trending towards continental crust composition as obvious in Fig. 7b. Therefore, the effect of continental curst contamination should be considered when discussing the petrogenesis and sources of the melts parental to the mafic dikes (see below).

5.1.2 Source of the mafic dikes

Compared with common basaltic rocks, the mafic dikes have relatively high SiO_2 (50.35-56.44 wt.%), but low MgO (3.54-5.34 wt.%), Cr (30.18-95.02 ppm), Ni (14.02-42.78 ppm) and $Mg^{\#}$ (0.47-0.54), indicative of their highly evolved nature from their mantle-derived parental melts through fractional crystallization dominated by olivine and clinopyroxene with, to some extent, crustal contamination (see above). Plagioclase fractionation is insignificant with an apparently weak negative Eu anomaly (Fig. 7a; Table 3).

In general, most basalts are evolved from asthenosphere-derived primitive melts. The asthenosphere is in general depleted in incompatible elements or depleted mantle (DM), but it is variably heterogeneous which can be variably enriched on all scales or enriched mantle (EM). Mid-ocean ridge basalts (MORB) are widely accepted as derived from the DM with depleted incompatible elements and depleted radiogenic

isotopic signatures interpreted to have resulted from continental crust extraction in Earth's early history (Gast, 1968; Niu and O'Hara, 2009). In comparison, the EM is complementarily enriched in incompatible elements and can generate magmas in diverse tectonic settings including plate boundaries and interiors (Anderson, 1981). The EM has variably high $^{87}Sr/^{86}Sr$, low $^{143}Nd/^{144}Nd$ and high $^{207}Pb/^{204}Pb$, $^{208}Pb/^{204}Pb$ at a given $^{206}Pb/^{204}Pb$ (Rollinson, 1993). Sun and McDonough (1989) suggest that the EM is characterized by $^{87}Sr/^{86}Sr \geqslant 0.7040$, $^{206}Pb/^{204}Pb < 18.6$ for EMI and 18.6-19.7 for EMII. Relatively high $^{87}Sr/^{86}Sr$ (0.7076-0.7104), $^{206}Pb/^{204}Pb$ (18.8-18.9) and low $\varepsilon_{Nd(t)}$ (-2.18 to -3.46) for the mafic dikes are consistent with their derivation from an EM source. Indeed, the Sr-Nd-Hf-Pb isotope (Figs. 8, 9), major element (Figs. 5, 6) and trace element (Fig. 7) compositions indicate that the primitive magmas parental to these mafic dikes are alkaline basalts derived from mantle sources enriched in incompatible elements and likely more enriched than OIB sources (Fig. 7). While the elevated abundances of Rb, U and Pb and relative depletion in Nb, Ta and Ti of these mafic dikes may have been affected by crustal contamination (see above), it is likely that much of these as well as the overall incompatible element enriched signatures may have largely inherited from enriched sources. With the exception of subduction-zone magmatism, melting of asthenospheric mantle will not produce melts with apparent Nb-Ta-Ti depletion, yet subduction-zone magmatism will produce melts with significantly more depleted Nb-Ta-Ti. However, melting of SCLM metasomatized in a mantle wedge environment (with terrestrial sediment input) can produce alkaline basalts parental to the mafic dikes (Huang et al., 2010; Zhao et al.,

2009). Indeed, this interpretation is consistent with the isotopic compositions of these mafic dikes falling with those of SCLM (e.g., $^{87}Sr/^{86}Sr$ of 0.7035-0.7100 and ε_{Nd} of +12 to -7; McDonough et al., 1985). Fig. 9a shows that on the Th/Nb-La/Nb plot (Plank, 2005), most mafic dikes have similar Th/Nb and La/Nb to OIB with a weak arc basaltic signature (i.e., low Nb, hence relatively high Th/Nb and La/Nb), which is in fact consistent with crustal assimilation (see above) or melting of metasomatized mantle lithosphere with sediment input (see above). All these together with the enriched Hf and Nd isotopes (Fig. 9b) manifest that the source of the mafic dikes is similar to that of OIB of metasomatic enrichment origin (Niu, 2008; Niu and O'Hara, 2003; Niu et al., 2002; Niu et al., 2012; Pilet et al., 2008). However, the weak arc-like or continental crust signature (e.g., Nb-Ta-Ti depletion) is consistent with the metasomatism taking place in the mantle wedge setting (Donnelly et al., 2004).

If the continental collision for the EKOB indeed ended in the Early Triassic (Yang et al., 2009), then the EKOB (sub-) volcanism would be considered as taking place in an intra-plate setting. It is yet unknown if such intra-plate magmatism was related to any sort of mantle plumes or post-collisional extension or orogenic collapse because conceptually all of these alternatives could cause asthenospheric upwelling, decompression melting, induced melting of prior metasomatized mantle lithosphere (e.g., during subduction episode) or even crustal melting (see below). We consider that it is immature at present to make any solid conclusion on this matter without further research. However, we can suggest that post-collisional extension (and related orogenic collapse) is a reasonable hypothesis to be tested in future studies. This is

because post-collisional magmatism can continue ~ 55 Myrs after continental collision, e.g., in southern Tibet (see Liu et al., 2014b; Zhao et al., 2009).

5.2. Origin of the felsic volcanic rocks

Given the differences of mafic dike and felsic volcanic rock samples in time and space, they are unlikely related to one another by fractional crystallization although the major element oxides show expected first-order trends except for Na_2O in SiO_2 variation diagrams (Fig. 6). Distinct isotopic compositions and different ratios of similarly incompatible elements (e.g. Nb/Th and Ta/U) of mafic and felsic rocks (Fig. 8) also preclude their genetic link through fractional crystallization.

The strongly fractionated LREE/HREE ratios ($[La/Yb]_N$ = 5.71 to 17.00) imply a partial-melting origin for the felsic volcanic rocks. Magmas derived by anatexis of continental crust typically have high $^{87}Sr/^{86}Sr$ ratios and low Sr contents (Hawkesworth and Vollmer, 1979). They preserve or increase the LILE/HFSE ratios of Rb/Nb and Rb/Zr during crustal anatexis, as Rb is more incompatible than Nb and Zr (Peccerillo et al., 2003). High $^{87}Sr/^{86}Sr$ (0.7213 to 0.7550), low Sr contents (25.46 to 295 ppm), and positive trends in Fig. 11a and b of the felsic volcanic rocks are all in favor of the crustal origin. In addition, during magma evolution from their respective parental melts, plagioclase is a dominated crystallization phase, and with increasing extent of fractional crystallization SiO_2 increases while Sr and Eu (hence Sr/Sr^* and Eu/Eu^*) decrease in the melt as a result, leading to the negative correlations of Sr/Sr^* and Eu/Eu* with SiO_2 (Figs. 11c, d). This interpretation is also consistent

with the SiO_2 co-variations with all other major elements (Fig. 6). It should be noted that the reverse of these correlations could also result from plagioclase presence as a residual phase during crustal melting. That is, one can prefer one possibility over another, but the interpretation is actually not unique, and both may actually be important.

In order to distinguish in which continental crust level the melts parental to the felsic volcanic rocks generated, the felsic rocks are compared with average composition of the upper (UCC) and lower (LCC) continental crust in Figure 7. They present almost identical patterns with the UCC expect for Eu, Sr and P (Fig. 7c, d), which are more depleted because of their more evolved nature with greater extent of plagioclase and apatite crystallization/removal. Upper crustal Zr/Y (8.3) and Sm/Nd (0.18) (Zr/Y = 9.19, Sm/Nd = 0.174 [UCC] vs. Zr/Y = 4.25, Sm/Nd = 0.255 [LCC]; Rudnick and Gao, 2003) further favour the genetic connection of the felsic volcanic rocks with the UCC. More importantly, the felsic volcanic rocks show Ta* and Nb* closely resemble those of the UCC, but significantly differ from the LCC (Fig. 10). This is because the lower crustal granulite rocks are depleted in U (relative to Ta and Th) and thus have the highest Th/U of 6.0 (vs. 3.9 [upper crust] and 4.3 [bulk crust]) and Ta/U of 3.0 (vs. 0.33 [upper crust] and 0.54 [bulk crust]) (Rudnick and Gao, 2003). This could suggest the upper crustal melting, but melting and melt segregation may actually take place in the lower crust with the melt emplaced in the upper crust undergoing varying extent of fractionation towards the observed felsic volcanic rocks. Felsic granulites in the LCC, which have been proved to be widespread and share

larger proportions (vs. mafic granulites) (Hans Wedepohl, 1995; Liu et al., 1996; Liu et al., 2001), may make main contributions to the felsic volcanic rocks at the deeper level when mafic magmas underplated from blow. However, it is worth noting that the felsic volcanic rocks are isotopically more depleted than the UCC with higher $\varepsilon_{Nd(t)}$ (-3.84 to -5.09) and lower I_{Sr} (0.7083-0.7097) (Figs. 8d, 9d) while displaying overlapping Nd-Hf isotopic compositions with the high Nb-Ta rhyolites and the mantle-derived mafic dikes (Fig. 8d and Fig. 9b, d; Ding et al., 2011). These observations require somewhat mixed sources to account for the petrogenesis of the felsic volcanic rocks. Apparently, mantle-derived alkaline basaltic melts parental to the mafic dikes must have been involved. Figure 9d plots various rocks from the EKOB in $\varepsilon_{Nd(t)}$ vs. I_{Sr} space. The late Triassic mafic dikes and felsic volcanic rocks fall in the range of intrusive igneous rocks derived from lithospheric mantle with input of crustal materials (see above).

With all the conceivable possibilities considered, we propose that the late Triassic mafic dikes represent melts evolved from alkaline basalts of metasomatized lithospheric mantle origin. Such mantle derived melts underplate and intrude the deep crust as juvenile crustal material. Partial melting of such juvenile crustal material produced felsic melts parental to the felsic volcanic rocks in the EKOB. That is, many of the original materials were derived directly (alkaline melts parental to the mafic dikes) or indirectly (felsic volcanic rocks) from the mantle in no distant past with varying extent of prior crustal contributions (i.e., subducted terrestrial sediments for metasomatizing the mantle lithosphere, deep crustal melting/assimilation and upper

crustal contamination etc.). In Figure 12, we attempt to estimate the relative proportions of crust and mantle contributions to the petrogenesis of mafic dikes and felsic volcanic rocks in terms of Sr and Nd isotopes. We choose two end members: (1) OIB-like basalts from the Zhiduo and Zaduo areas as representing the contemporary Paleo-Tethyan mantle component (Ma et al., 2007); (2) Jinshuikou cordierite granites from northeastern margin of the Tibetan plateau as representing the upper continental crust (Ba et al., 2012). The calculations show that isotopically, the felsic volcanic rocks represent mixing (melting and melt hybridization) of 45-50% crustal materials and 50-55% mantle-derived alkaline mafic melts (Fig. 12). If the latter is parental to the mafic dikes, then these dikes represent hybridization of ~ 65% of mantle materials and ~ 35% mature crustal materials.

The above is conceptually important for understanding the origin of the juvenile crust and continental crustal accretion through magmatism in the broad context of the orogenesis from seafloor subduction to continental collision and to post-collisional processes (see Niu et al., 2013 for review).

5.3. Tectonic significance

The paleo-ocean recorded by the EKOB underwent poly-cycle tectonic evolution (Yin and Zhang, 1997), among which the opening-closing cycle of the A'nyemaqen Ocean from the late Paleozoic to early Mesozoic was the latest tectonic event (Jiang et al., 1992; Mo et al., 2007). Along with the A'nyemaqen Ocean closing, active magmatism occurred and formed abundant granitoids constituting the main body of

the EKOB (Jiang et al., 1992; Li et al., 2013b; Mo et al., 2007). We consider the late Triassic mafic dikes from the EKOB were derived from the metasomatized subcontinental lithospheric mantle in response to post-collisional processes, whose nature remains unclear and requires further research, but we hypothesize the significance of asthenospheric upwelling, decompression melting, induced melting of metasomatized mantle lithosphere. Such mantle-derived alkaline basaltic melts are parental to the mafic dikes in the EKOB. Underplating and intrusion of such melts in the deep crust represent juvenile crustal material, whose melting produced the felsic volcanic rocks. We further hypothesize that much of the volumetrically significant contemporary granitoids, including the A-type granite, likely represent different products of the same thermal event (Hu et al., in preparation).

The timing of A'nyemaqen Ocean closing and continental collision is thought to be the early to middle Triassic (Pan et al., 2012; Xia et al., 2014; Yang et al., 2009) or late Triassic (Guo et al., 1998; Liu et al., 1984; Luo et al., 2002; Mo et al., 2007). Hence, the late Triassic volcanism in particular and the large scale granitoid magmatism in general in the EKOB are associated with post-collisional processes. Mantle plumes (Chung and Jahn, 1995; Hoek and Seitz, 1995; Lightfoot et al., 1993; Srivastava, 2011; Stepanova and Stepanov, 2010), slab break-off (Blanckenburg and Davies, 1995; Caprarelli and Leitch, 2001; Davies and von Blanckenburg, 1995; Maury et al., 2000; Xu et al., 2008) and convective lithosphere removal (Corrigan and Hanmer, 1997; Hoernle et al., 2006; Tatsumi and Kimura, 1991; Turner et al., 1996; Williams et al., 2001) are popular interpretations for asthenospheric upwelling and

related magmatism, but we consider that post-collisional lithosphere extension and orogenic collapse are most likely the major cause to consider, which is in nature a hypothesis to be tested.

6. Conclusion

1. The mafic dikes (diabase) and felsic volcanic rocks (rhyolitic tuff and rhyolite porphyry) from the EKOB synchronously emplaced in the late Triassic (from 228 to 218 Ma).
2. Geochemical data suggest that most of the mafic dikes in the EKOB are highly evolved alkaline basaltic rocks. Their parental melts were likely derived from subcontinental lithospheric mantle metasomatized in a mantle wedge environment (with terrestrial sediment input). Crustal contamination is also important and the overall contribution of mature crustal materials may be up to ~ 35%.
3. The felsic volcanic rocks were generated from mixing (melting and melt hybridization) of 45-50% crustal materials and 50-55% mantle-derived alkaline mafic melts represented by the mafic dikes. Such mantle-derived melts underplated and intruded the deep crust as juvenile crustal materials. Partial melting of such juvenile crustal materials produced felsic melts parental to the felsic volcanic rocks in the EKOB.
4. We consider that the late Triassic mafic dikes and felsic volcanic rocks are associated with post-collisional extension and related orogenic collapse. Such processes are most likely and significant to cause asthenospheric upwelling,

decompression melting and induced melting of prior metasomatized mantle lithosphere (e.g., during subduction episode) or even crustal melting. It is conceptually important for understanding the origin of the juvenile crust and continental crustal accretion through magmatism in the broad context of orogenesis from seafloor subduction to continental collision and to post-collisional processes.

Acknowledgements

This work is supported by NSFC grants (41130314, 91014003), and grants by the Chinese Academy of Sciences, Shandong Province and the City of Qingdao to Yaoling Niu. We thank Zhenxing Hu, Yuxin Ma, Wenli Sun, Jinju Liu and Huixia Cui for help with sample preparation, and Lian Zhou, Jianxin Zhao, Yuexing Feng, Pengyuan Guo and Pu Sun for assistance with isotope analysis. We also thank Di-Cheng Zhu (guest editor) and the two anonymous reviewers for their detailed and constructive comments.

References

Anderson D. L., 1981. Hotspots, Basalts, and the Evolution of the Mantle. Science 213, 82-89.

Ba, J., Chen, N.S., Wang, Q.Y., Wang, X.Y., Zhang, L., Wang, S.Q., 2012. Nd-Sr-Pb isotopic compositions of cordierite granite on southern margin of the qaidam block, NW China, and constraints on its petrogenesis, tectonic affinity of source region and tectonic implications. Earth Science-Journal of China University of Geosciences, 80-92 (in Chinese with English abstract).

Belousova, E., Griffin, W., O'Reilly, S.Y., Fisher, N., 2002. Igneous zircon: trace element composition as an indicator of source rock type. Contributions to Mineralogy and Petrology 143, 602-622.

Blanckenburg, F., Davies, J.H., 1995. Slab breakoff: a model for syncollisional magmatism and tectonics in the Alps. Tectonics 14, 120-131.

Buchan, K.L., Mortensen, J.K., Card, K.D., Percival, J.A., 1998. Paleomagnetism and U-Pb geochronology of diabase dyke swarms of Minto block, Superior Province, Quebec, Canada. Canadian Journal of Earth Sciences 35, 1054-1069.

Caprarelli, G., Leitch, E.C., 2001. Geochemical evidence from Lower Permian volcanic rocks of northeast New South Wales for asthenospheric upwelling following slab breakoff. Australian Journal of Earth Sciences 48, 151-166.

Chen, L., Ma, C.Q., Zhang, J.Y., Mason, R., Zhang, C., 2011. Mafic dykes derived from Early Cretaceous depleted mantle beneath the Dabie orogenic belt: implications for changing lithosphere mantle beneath Eastern China. Geological Journal 46, 333-343.

Christiansen, E.H., Burt, D.M., Sheridan, M.F., Wilson, R.T., 1983. The petrogenesis of topaz rhyolites from the western United States. Contributions to Mineralogy

and Petrology 83, 16-30.

Chung, S.L., Jahn, B.M., 1995. Plume-lithosphere interaction in generation of the Emeishan flood basalts at the Permian-Triassic boundary. Geology 23, 889-892.

Corfu, F., Hanchar, J.M., Hoskin, P.W.O., Kinny, P., 2003. Atlas of Zircon Textures. Reviews in Mineralogy and Geochemistry 53, 469-500.

Corrigan, D., Hanmer, S., 1997. Anorthosites and related granitoids in the Grenville orogen: A product of convective thinning of the lithosphere? Geology 25, 61-64.

Davies, J.H., von Blanckenburg, F., 1995. Slab breakoff: a model of lithosphere detachment and its test in the magmatism and deformation of collisional orogens. Earth and Planetary Science Letters 129, 85-102.

Deniel, C., Pin, C., 2001. Single-stage method for the simultaneous isolation of lead and strontium from silicate samples for isotopic measurements. Analytica Chimica Acta 426, 95-103.

Ding, S., Huang, H., Niu, Y.L., Zhao, Z.D., Yu, X.H., Mo, X.X., 2011. Geochemistry, geochronology and petrogenesis of East Kunlun high Nb-Ta rhyolites. Acta Petrologica Sinica 27, 3603-3614 (in Chinese with English abstract).

Donnelly, K.E., Goldstein, S.L., Langmuir, C.H., Spiegelman, M., 2004. Origin of enriched ocean ridge basalts and implications for mantle dynamics. Earth and Planetary Science Letters 226, 347-366.

Gast P. W., 1968. Trace element fractionation and the origin of tholeiitic and alkaline magma types. Geochimica et Cosmochimica Acta 32, 1057-1086.

Goldberg, A.S., 2010. Dyke swarms as indicators of major extensional events in the

1.9–1.2Ga Columbia supercontinent. Journal of Geodynamics 50, 176-190.

Goldstein, S.J., Jacobsen, S.B., 1988. Nd and Sr isotopic systematics of river water suspended material: implications for crustal evolution. Earth and Planetary Science Letters 87, 249-265.

Guo, P.Y., Niu, Y.L., Ye, L., Liu, J.J., Sun, P., Cui, H.X., Zhang, Y., Gao, J.P., Su, L., Zhao, J.X., Feng, Y.X., 2014. Lithosphere thinning beneath west North China Craton: Evidence from geochemical and Sr–Nd–Hf isotope compositions of Jining basalts. Lithos 202-203, 37-54.

Guo, Z.F., Deng, J.F., Xu, Z.Q., Mo, X.X., Luo, Z.H., 1998. Late Paleozoic-Mesozoic intracontinental orogenic process and intermedate-acidic igneous rocks from the Eastern Kunlun Mountains from Northwestern China. Geoscience, 51-59 (in Chinese with English abstract).

Hans Wedepohl, K., 1995. The composition of the continental crust. Geochimica et Cosmochimica Acta 59, 1217-1232.

Harris, N., Xu, R.H., Lewis, C., Hawkesworth, C., Zhang, Y.Q., 1988. Isotope geochemistry of the 1985 Tibet geotraverse, Lhasa to Golmud. Philosophical Transactions of the Royal Society of London. Series A, Mathematical and Physical Sciences 327, 263-285.

Hawkesworth, C.J., Vollmer, R., 1979. Crustal contamination versus enriched mantle: $^{143}Nd/^{144}Nd$ and $^{87}Sr/^{86}Sr$ evidence from the Italian volcanics. Contributions to Mineralogy and Petrology 69, 151-165.

Hoek, J.D., Seitz, H.M., 1995. Continental mafic dyke swarms as tectonic indicators:

an example from the Vestfold Hills, East Antarctica. Precambrian Research 75, 121-139.

Hoernle, K., White, J.D.L., van den Bogaard, P., Hauff, F., Coombs, D.S., Werner, R., Timm, C., Garbe-Schönberg, D., Reay, A., Cooper, A.F., 2006. Cenozoic intraplate volcanism on New Zealand: Upwelling induced by lithospheric removal. Earth and Planetary Science Letters 248, 350-367.

Hoskin, P.W.O., Schaltegger, U., 2003. The composition of zircon and igneous and metamorphic petrogenesis. Mineralogical Society of America, Washington, DC, ETATS-UNIS, p. 36.

Huang, X.L., Niu, Y.L., Xu, Y.G., Chen, L.L., Yang, Q.J., 2010. Mineralogical and geochemical constraints on the petrogenesis of post-collisional potassic and ultrapotassic rocks from western Yunnan, SW China. Journal of Petrology 51, 1617-1654.

Huppert, H.E., Sparks, R.S.J., 1988. The generation of granitic magmas by intrusion of basalt into continental crust. Journal of Petrology 29, 599-624.

Irvine, T.N., Baragar, W.R.A., 1971. A guide to the chemical classification of the common volcanic rocks. Canadian Journal of Earth Sciences 8, 523-548.

Jiang, C.F., Yang, J.S., Feng, B.G., Zhu, Z.Z., Zhao, M., Chai, Y.C., Shi, X.D., Wang, H.D., Hu, J.Q., 1992. Opening-closing tectonics of Kunlun Mountains. Series of geological memoirs 5, 1-224 (in Chinese with English abstract).

Le Bas, M., Le Maitre, R., Streckeisen, A., Zanettin, B., 1986. A chemical classification of volcanic rocks based on the total alkali-silica diagram. Journal of

Petrology 27, 745-750.

Li, R.B., Pei, X.Z., Li, Z.C., Sun, Y., Feng, J.Y., Pei, L., Chen, G.C., Liu, C.J., Chen, Y.X., 2013a. Geochemical Features, Age, and Tectonic Significance of the Kekekete Mafic-ultramafic Rocks, East Kunlun Orogen, China. Acta Geologica Sinica - English Edition 87, 1319-1333.

Li, W., Neubauer, F., Liu, Y.J., Genser, J., Ren, S.M., Han, G.Q., Liang, C.Y., 2013b. Paleozoic evolution of the Qimantagh magmatic arcs, Eastern Kunlun Mountains: Constraints from zircon dating of granitoids and modern river sands. Journal of Asian Earth Sciences 77, 183-202.

Lightfoot, P.C., Hawkesworth, C.J., Hergt, J., Naldrett, A.J., Gorbachev, N.S., Fedorenko, V.A., Doherty, W., 1993. Remobilisation of the continental lithosphere by a mantle plume: major-, trace-element, and Sr-, Nd-, and Pb-isotope evidence from picritic and tholeiitic lavas of the Noril'sk District, Siberian Trap, Russia. Contributions to Mineralogy and Petrology 114, 171-188.

Liu, B., Ma, C.Q., Zhang, J.Y., Xiong, F.H., Huang, J., Jiang, H.A., 2014a. 40Ar–39Ar age and geochemistry of subduction-related mafic dikes in northern Tibet, China: petrogenesis and tectonic implications. International Geology Review 56, 57-73.

Liu, D., Zhao, Z.D., Zhu, D.C., Niu, Y.L., DePaolo, D.J., Harrison, T.M., Mo, X.X., Dong, G.C., Zhou, S., Sun, C.G., 2014b. Postcollisional potassic and ultrapotassic rocks in southern Tibet: Mantle and crustal origins in response to India–Asia collision and convergence. Geochimica et Cosmochimica Acta 143, 207-231.

Liu, L., Zhou, D.W., Wang, Y., Chen, D.L., Liu, Y., 1996. Study and implication of the high-pressure felsic granulite in the Qinling complex of East Qinling. Science in China (Series D) 26, 56-63 (in Chinese with English abstract).

Liu, S., Hu, R.Z., Gao, S., Feng, C.X., Feng, G.Y., Qi, Y.Q., Coulson, I.M., Yang, Y.H., Yang, C.G., Tang, L., 2012. Geochemical and isotopic constraints on the age and origin of mafic dikes from eastern Shandong Province, eastern North China Craton. International Geology Review 54, 1389-1400.

Liu, Y.S., Gao, S., Hu, Z.C., Gao, C.G., Zong, K.Q., Wang, D.B., 2010a. Continental and Oceanic Crust Recycling-induced Melt-Peridotite Interactions in the Trans-North China Orogen: U-Pb Dating, Hf Isotopes and Trace Elements in Zircons from Mantle Xenoliths. Journal of Petrology 51, 537-571.

Liu, Y.S., Gao, S., Yuan, H.L., Zhou, L., Liu, X.M., Wang, X.C., Hu, Z.C., Wang, L.S., 2004. U–Pb zircon ages and Nd, Sr, and Pb isotopes of lower crustal xenoliths from North China Craton: insights on evolution of lower continental crust. Chemical Geology 211, 87-109.

Liu, Y.S., Gao, S., Zhou, L., Zhang, L., Jin, S.Y., 2001. Geochronology and geodynamic implications of the felsic granulite xenoliths from the Hannuoba basalt. Geochimica 30, 50.

Liu, Y.S., Hu, Z.C., Zong, K.Q., Gao, C.G., Gao, S., Xu, J., Chen, H.H., 2010b. Reappraisement and refinement of zircon U-Pb isotope and trace element analyses by LA-ICP-MS. Chinese Science Bulletin 55, 1535-1546.

Liu, Z.Q., Liu, B.T., Zheng, H.X., Jiang, C.F., 1984. New Thoughts on the geology of

Tethys-Himalayan tectonic domain. Contribution to the Geology of the Qinghai-Xizang (TIBET) Plateau, 131-146 (in Chinese with English abstract).

Ludwig, K.R., 2003. Isoplot 3.00: A geochronological toolkit for Microsoft Excel. Berkeley Geochronology Center, Berkeley, California.

Luo, Z.H., Ke, S., Cao, Y.Q., Deng, J.F., Chen, H.W., 2002. Late Indosinian mantle derived magmatism in the East Kunlun. Geological Bulletin of China, 292-297 (in Chinese with English abstract).

Míková, J., Denková, P., 2007. Modified chromatographic separation scheme for Sr and Nd isotope analysis in geological silicate samples. Journal of Geosciences 52, 221-226.

Ma, L.Y., Niu, Z.J., Bai, Y.S., Duan, Q.F., Wang, J.X., 2007. Sr, Nd and Pb isotopic geochemistry of Permian volcanic rocks from southern Qinghai and their geological significance. Earth Science—Journal of China University of Geosciences 32, 22-28 (in Chinese with English abstract).

Maury, R.C., Fourcade, S., Coulon, C., Bellon, H., Coutelle, A., Ouabadi, A., Semroud, B., Megartsi, M.h., Cotten, J., Belanteur, O., 2000. Post-collisional Neogene magmatism of the Mediterranean Maghreb margin: a consequence of slab breakoff. Comptes Rendus de l'Académie des Sciences-Series IIA-Earth and Planetary Science 331, 159-173.

McDonough, W.F., McCulloch, M.T., Sun, S.S., 1985. Isotopic and geochemical systematics in Tertiary-Recent basalts from southeastern Australia and implications for the evolution of the sub-continental lithosphere. Geochimica et

Cosmochimica Acta 49, 2051-2067.

Mo, X.X., Luo, Z.H., Deng, J.F., Yu, X.H., Liu, C.D., Chen, H.W., Yuan, W.M., Liu, Y.H., 2007. Granitoids and Crustal Growth in the East-Kunlun Orogenic Belt. Geological Journal of China Universities, 403-414 (in Chinese with English abstract).

Niu, Y.L., Zhao, Z.D., Zhu, D.C., Mo, X.X., 2013. Continental collision zones are primary sites for net continental crust growth—A testable hypothesis. Earth-Science Reviews 127, 96-110.

Niu, Y.L., 2008. The origin of alkaline lavas. Science 320, 883.

Niu, Y.L., Batiza, R., 1997. Trace element evidence from seamounts for recycled oceanic crust in the Eastern Pacific mantle. Earth and Planetary Science Letters 148, 471-483.

Niu, Y.L., O'Hara, M.J., 2003. Origin of ocean island basalts: A new perspective from petrology, geochemistry, and mineral physics considerations. Journal of Geophysical Research: Solid Earth 108, 2209.

Niu, Y.L., O'Hara, M.J., 2009. MORB mantle hosts the missing Eu (Sr, Nb, Ta and Ti) in the continental crust: New perspectives on crustal growth, crust–mantle differentiation and chemical structure of oceanic upper mantle. Lithos 112, 1-17.

Niu, Y.L., Regelous, M., Wendt, I.J., Batiza, R., O'Hara, M.J., 2002. Geochemistry of near-EPR seamounts: importance of source vs. process and the origin of enriched mantle component. Earth and Planetary Science Letters 199, 327-345.

Niu, Y.L., Wilson, M., Humphreys, E.R., O'Hara, M.J., 2012. A trace element

perspective on the source of ocean island basalts (OIB) and fate of subducted ocean crust (SOC) and mantle lithosphere (SML). Episodes 35, 310-327.

Pan, G.T., Wang, L.Q., Li, R.S., Yuan, S.H., Ji, W.H., Yin, F.G., Zhang, W.P., Wang, B.D., 2012. Tectonic evolution of the Qinghai-Tibet Plateau. Journal of Asian Earth Sciences 53, 3-14.

Pan, Y.S., Zhou, W.M., Xu, R.H., Wang, D.A., Zhang, Y.Q., Xie, Y.W., Chen, T.E., Luo, H., 1996. Geological characteristics and evolution of the Kunlun Mountains region during the early Paleozoic. Science in China (Series D) 4, 337-347.

Pearce, J.A., Norry, M.J., 1979. Petrogenetic implications of Ti, Zr, Y, and Nb variations in volcanic rocks. Contributions to Mineralogy and Petrology 69, 33-47.

Peccerillo, A., Barberio, M.R., Yirgu, G., Ayalew, D., Barbierl, M., Wu, T.W., 2003. Relationships between Mafic and Peralkaline Silicic Magmatism in Continental Rift Settings: a Petrological, Geochemical and Isotopic Study of the Gedemsa Volcano, Central Ethiopian Rift. Journal of Petrology 44, 2003-2032.

Pilet, S., Baker, M.B., Stolper, E.M., 2008. Metasomatized lithosphere and the origin of alkaline lavas. Science 320, 916-919.

Pin, C., Zalduegui, J.S., 1997. Sequential separation of light rare-earth elements, thorium and uranium by miniaturized extraction chromatography: Application to isotopic analyses of silicate rocks. Analytica Chimica Acta 339, 79-89.

Plank, T., 2005. Constraints from Thorium/Lanthanum on Sediment Recycling at Subduction Zones and the Evolution of the Continents. Journal of Petrology 46,

921-944.

Ratajeski, K., Glazner, A.F., Miller, B.V., 2001. Geology and geochemistry of mafic to felsic plutonic rocks in the Cretaceous intrusive suite of Yosemite Valley, California. Geological Society of America Bulletin 113, 1486-1502.

Ren, J.H., Liu, Y.Q., Zhou, D.W., Feng, Q., Zhang, K., Dong, Z.L., Qin, P.L., 2010. Geochemical characteristics and LA-ICP-MS zircon U-Pb dating of basic dykes in the Xiaomiao area, East Kunlun. Journal of Jilin University (Earth Science Edition), 859-868 (in Chinese with English abstract).

Rickwood, P.C., 1989. Boundary lines within petrologic diagrams which use oxides of major and minor elements. Lithos 22, 247-263.Rollinson, H., 1993. Using Geochemical Data: Evaluation, Interpretation, Presentation. Longman, New York.

Rudnick, R.L., Gao, S., 2003. Composition of the continental crust. Treatise on Geochemistry 3, 1-64.

Salters, V.J.M., White, W.M., 1998. Hf isotope constraints on mantle evolution. Chemical Geology 145, 447-460.

Shao, F.L., Niu, Y.L., Regelous, M., Zhu, D.C., 2015. Petrogenesis of peralkaline rhyolites in an intra-plate setting: Glass House Mountains, southeast Queensland, Australia. Lithos 216, 196-210.

Song, B., Zhang, Y.H., Wan, Y.S., Jian, P., 2002. Mount making and procedure of SHRMP dating. Geological Review, 26-30 (in Chinese with English abstract).

Song, S.G., Su, L., Li, X.H., Zhang, G.B., Niu, Y.L., Zhang, L.F., 2010. Tracing the 850-Ma continental flood basalts from a piece of subducted continental crust in

the North Qaidam UHPM belt, NW China. Precambrian Research 183, 805-816.

Srivastava, R.K., 2011. Dyke Swarms: Keys for Geodynamic Interpretation. Springer, Heidelberg, 1-603.

Stepanova, A., Stepanov, V., 2010. Paleoproterozoic mafic dyke swarms of the Belomorian Province, eastern Fennoscandian Shield. Precambrian Research 183, 602-616.

Sun, S.-s., McDonough, W.F., 1989. Chemical and isotopic systematics of oceanic basalts: implications for mantle composition and processes. Geological Society, London, Special Publications 42, 313-345.

Takanashi, K., Shuto, K., Sato, M., 2011. Origin of Late Paleogene to Neogene basalts and associated coeval felsic volcanic rocks in Southwest Hokkaido, northern NE Japan arc: Constraints from Sr and Nd isotopes and major- and trace-element chemistry. Lithos 125, 368-392.

Tatsumi, Y., Kimura, N., 1991. Secular variation of basalt chemistry in the Kenya Rift: Evidence for the pulsing of asthenospheric upwelling. Earth and Planetary Science Letters 104, 99-113.

Tian, W., Campbell, I.H., Allen, C.M., Guan, P., Pan, W.Q., Chen, M.M., Yu, H.J., Zhu, W.P., 2010. The Tarim picrite–basalt–rhyolite suite, a Permian flood basalt from northwest China with contrasting rhyolites produced by fractional crystallization and anatexis. Contributions to Mineralogy and Petrology 160, 407-425.

Turner, S., Arnaud, N., Liu, J., Rogers, N., Hawkesworth, C., Harris, N., Kelley, S.,

Van Calsteren, P., Deng, W., 1996. Post-collision, Shoshonitic Volcanism on the Tibetan Plateau: Implications for Convective Thinning of the Lithosphere and the Source of Ocean Island Basalts. Journal of Petrology 37, 45-71.

Turner, S.P., Foden, J.D., Morrison, R.S., 1992. Derivation of some A-type magmas by fractionation of basaltic magma: An example from the Padthaway Ridge, South Australia. Lithos 28, 151-179.

Williams, H., Turner, S., Kelley, S., Harris, N., 2001. Age and composition of dikes in Southern Tibet: New constraints on the timing of east-west extension and its relationship to postcollisional volcanism. Geology 29, 339-342.

Xia, R., Wang, C.M., Deng, J., Carranza, E.J.M., Li, W.L., Qing, M., 2014. Crustal thickening prior to 220Ma in the East Kunlun Orogenic Belt: Insights from the Late Triassic granitoids in the Xiao-Nuomuhong pluton. Journal of Asian Earth Sciences 93, 193-210.

Xiong, F.H., Ma, C.Q., Jiang, H.A., Liu, B., Huang, J., 2014a. Geochronology and geochemistry of Middle Devonian mafic dykes in the East Kunlun orogenic belt, Northern Tibet Plateau: Implications for the transition from Prototethys to Paleotethys orogeny. Chemie der Erde - Geochemistry 74, 225-235.

Xiong, F.H., Ma, C.Q., Jiang, H.A., Liu, B., Zhang, J.Y., Zhou, Q., 2013. Petrogenetic and tectonic significance of Permian calc-alkaline lamprophyres, East Kunlun orogenic belt, Northern Qinghai-Tibet Plateau. International Geology Review 55, 1817-1834.

Xiong, F.H., Ma, C.Q., Zhang, J.Y., Liu, B., Jiang, H.A., 2014b. Reworking of old

continental lithosphere: an important crustal evolution mechanism in orogenic belts, as evidenced by Triassic I-type granitoids in the East Kunlun orogen, Northern Tibetan Plateau. Journal of the Geological Society.

Xiu, Q.Y., Yin, Y.J., Li, H.M., 2001. Sampling and Mineral Sorting for Single Zircon U-Pb Dating. Progress in Precambrian Research, 107-110 (in Chinese with English abstract).

Xu, Y.G., Lan, J.B., Yang, Q.J., Huang, X.L., Qiu, H.N., 2008. Eocene break-off of the Neo-Tethyan slab as inferred from intraplate-type mafic dykes in the Gaoligong orogenic belt, eastern Tibet. Chemical Geology 255, 439-453.

Yang, J.H., Wu, F.Y., Wilde, S.A., Chen, F.K., Liu, X.M., Xie, L.W., 2008. Petrogenesis of an Alkali Syenite–Granite–Rhyolite Suite in the Yanshan Fold and Thrust Belt, Eastern North China Craton: Geochronological, Geochemical and Nd–Sr–Hf Isotopic Evidence for Lithospheric Thinning. Journal of Petrology 49, 315-351.

Yang, J.S., Robinson, P.T., Jiang, C.F., Xu, Z.Q., 1996. Ophiolites of the Kunlun Mountains, China and their tectonic implications. Tectonophysics 258, 215-231.

Yang, J.S., Shi, R.D., Wu, C.L., Wang, X.B., Robinson, P., 2009. Dur'ngoi ophiolite in East Kunlun, Northeast Tibetan plateau: Evidence for paleo-Tethyan suture in Northwest China. Journal of Earth Science 20, 303-331.

Yang, Y.H., Zhang, H.F., Chu, Z.Y., Xie, L.W., Wu, F.Y., 2010. Combined chemical separation of Lu, Hf, Rb, Sr, Sm and Nd from a single rock digest and precise and accurate isotope determinations of Lu–Hf, Rb–Sr and Sm–Nd isotope systems

using Multi-Collector ICP-MS and TIMS. International Journal of Mass Spectrometry 290, 120-126.

Yin, A., Harrison, T.M., 2000. Geologic Evolution of the Himalayan-Tibetan Orogen. Annual Review of Earth and Planetary Sciences 28, 211-280.

Yin, H.F., Zhang, K.X., 1997. Characteristics of the Eastern Kunlun Orogenic Belt. Earth Science-Journal of China University of Geosciences, 3-6 (in Chinese with English abstract).

Yuan, W.M., Mo, X.X., Yu, X.H., Luo, Z.H., 2000. The Record of Indosinian Tectonic Setting from the Granotoid of Eastern kunlun mountains. Geological Review, 203-211 (in Chinese with English abstract).

Zhao, Z.D., Mo, X.X., Dilek, Y., Niu, Y.L., DePaolo, D.J., Robinson, P., Zhu, D.C., Sun, C.G., Dong, G.C., Zhou, S., 2009. Geochemical and Sr–Nd–Pb–O isotopic compositions of the post-collisional ultrapotassic magmatism in SW Tibet: petrogenesis and implications for India intra-continental subduction beneath southern Tibet. Lithos 113, 190-212.

Zhu, Y.H., Lin, Q.X., Jia, C.X., Wang, G.C., 2006. SHRIMP zircon U-Pb age and significance of Early Paleozoic volcanic rocks in East Kunlun orogenic belt, Qinghai Province, China. Science in China Series D 49, 88-96.

Captions

Fig. 1 (a) Outline of the geological framework of the Greater Tibetan Plateau with several sutures: IYS, Indus-Yarlung Zangbo suture; BNS, Bangong-Nujiang suture; JS, Jinsha suture; AKMS, A'nyemaqen-Kunlun-Mutztagh suture; SQS, South Qilian suture; DHS, Danghe Nan Shan suture; NQS, North Qilian suture (after Niu et al., 2013; Yin and Harrison, 2000). (b) Schematic geological map of the East Kunlun Orogenic Belt (EKOB) showing two major faults (Central Kunlun Fault and South Kunlun Fault) and corresponding zones, i.e., northern, middle and southern zones (after Jiang et al., 1992). (c) Simplified distribution map of intrusive (granitoids) and volcanic rocks (T_3e & T_3b) along the EKOB (modified from 1:1,000,000 geological map of northern Tibetan Plateau (Institute of Geology and Mineral Resources, Xi'an, China, 2006). The abbreviations beside the sample locations denote the Yeniugou area (YNG), Tufangzi area (QMX), Dulan area (DL) (Ding et al., 2011), Reshui area (RSX) and Yingde'er area (YDE), and the ages for sample locations are new data of this study except for the "DL" age from Ding et al. (2011).

Fig. 2 (a) Outcrop of diabasic dikes intruding the A-type granite in the East Kunlun Orogenic Belt. (b) Field photos of chilled margins in the mafic dikes (left) and the schematic illustration of their emplacement (right). When the hot mafic magmas [I] intruded the cold A-type granite, they were quenched and developed chilled margins at the contact with the granite. These dikes may serve as conduit for subsequent mafic magma [II] transport with chilled margins developed at the contact with [I] if [I] were

sufficiently cold (e.g., > 200°C cooler). Photomicrographs of the diabase (c), rhyolitic tuff (d) and rhyolite porphyry (e).

Fig. 3 Cathodoluminescence images of representative zircons from the diabase (a. YNG12-03), rhyolitic tuff (b. QMX12-01) and rhyolite porphyry (c. RSX12-48) of the late Triassic mafic dikes and felsic volcanic rocks from the East Kunlun Orogenic Belt. The circles with numbers are analysis spots of zircon U-Pb dating, indicating their ages (Ma) which are given in Table 2.

Fig. 4 Concordia diagrams of dated zircons from sample (a) YNG13-03 (diabase), (b) QMX12-01 (rhyolitic tuff) and (c) RSX12-48(rhyolite porphyry) of the late Triassic mafic dikes and felsic volcanic rocks from the East Kunlun Orogenic Belt.

Fig. 5 Total alkalis vs. SiO_2 (Le Bas et al., 1986) (a) and K_2O vs. SiO_2 (b) diagrams of the late Triassic mafic dikes and felsic volcanic rocks form the East Kunlun Orogenic Belt. The dashed alkaline-subalkaline division line is from Irvine and Baragar (1971). The compositional fields of tholeiitic (TH), low-K calc-alkaline (CA), high-K calc-alkaline (K-CA) and shoshonite (SH) rock series are from Rickwood (1989).

Fig. 6 SiO_2 variation diagrams of the late Triassic mafic dikes and felsic volcanic rocks from the East Kunlun Orogenic Belt.

Fig. 7 Normalized rare earth element (REE) and multi-element diagrams of the late Triassic mafic dikes and felsic volcanic rocks from the East Kunlun Orogenic Belt. Average ocean island basalts (OIB), bulk continental crust (BCC), upper continental crust (UCC) and lower continental crust (LCC) compositions are also plotted for comparison. Chondrite, primitive mantle and OIB data are from Sun and McDonough (1989). CC values are from Rudnick and Gao (2003).

Fig. 8 Nb/Th (a), Ta/U (b), $^{87}Sr/^{86}Sr$ (c) and $\varepsilon_{Nd(t)}$ (d) vs. SiO_2 diagrams of the late Triassic mafic dikes and felsic volcanic rocks from the East Kunlun Orogenic Belt. Except for the high Nb-Ta rhyolite (Ding et al., 2011), the weak negative Nb/Th, Ta/U and $\varepsilon_{Nd(t)}$ correlations with SiO_2 and the weak positive $^{87}Sr/^{86}Sr$ correlation with SiO_2 in mafic dikes (diabase) are consistent with crustal contamination during magma ascent. Average bulk continental crust (BCC) and upper continental crust (UCC) compositions are from Rudnick and Gao (2003). $^{87}Sr/^{86}Sr$ and $\varepsilon_{Nd(t)}$ data of the UCC are from Goldstein and Jacobsen (1988).

Fig. 9 (a) La/Nb vs. Th/Nb diagram, showing that the mafic dikes from the East Kunlun Orogenic Belt (EKOB) and OIB are similar with weak crustal assimilation, but differ from MORB and arc basalts (modified after Plank, 2005). (b) $\varepsilon_{Nd(0)}$ vs. $\varepsilon_{Hf(0)}$ diagram showing isotopically more enriched characteristics of the mafic dikes than MORB and even OIB (the latter data from Salters and White, 1998). (c) Zr vs. Zr/Y diagram, showing the mafic dikes plotting in the within-plate basalt field (after Pearce

and Norry, 1979; WPB, within plate basalts; MORB, mid-ocean ridge basalts; IAB, island arc basalts). Note that we plot the felsic volcanic rocks for comparison. (d) I_{Sr} vs. $\varepsilon_{Nd(t)}$ diagram of the late Triassic mafic dikes and felsic volcanic rocks from the EKOB. Isotopic fields compiled by Xiong et al. (2014b) are plotted for comparison (The high Nb-Ta rhyolites are not plotted due to their very low concentrations of Sr (Table 4), leading to extremely high and variable $^{87}Rb/^{86}Sr$ ratios and thus unrealistic $^{87}Sr/^{86}Sr$ ratios (I_{Sr}) (Ding et al., 2011).

Fig. 10 Diagram of Ta* vs. Nb* for the late Triassic mafic dikes and felsic volcanic rocks from the East Kunlun Orogenic Belt (after Niu and Batiza, 1997). Compared with common basalts, the diabasic dikes have Ta and Nb deficiencies, but significantly less so than continental crustal materials as well as the felsic volcanic rocks. These observations are consistent with the diabasic rocks gaining crustal contamination. Data of primitive mantle and average oceanic basalts (OIB, E-MORB, N-MORB) are from Sun and McDonough (1989). Crust composition (BCC, LCC, UCC) are from Rudnick and Gao (2003).

Fig. 11 Co-variation diagrams of SiO_2 and Rb with the abundances and ratios of other incompatible elements for the felsic volcanic rocks from the East Kunlun Orogenic Belt. (a), (b) Rb/Nb and Rb/Zr vs. Rb diagrams. Rb/Nb and Rb/Zr increase progressively with increasing Rb, implying an origin of crustal anatexis for the felsic volcanic rocks because magmas preserve or increase the LILE/HFSE ratios of Rb/Nb

and Rb/Zr during crustal anatexis (Peccerillo et al., 2003). (c), (d) Sr/Sr^* and Eu/Eu^* vs. SiO_2 diagrams showing the effect of plagioclase fractionation (see Table 3 for Sr/Sr^* and Eu/Eu^* calculation).

Fig. 12 Showing I_{Sr} and $\varepsilon_{Nd(t)}$ compositions of the late Triassic mafic dikes and felsic volcanic rocks from the East Kunlun Orogenic Belt, which could be explained by mixing between a Paleo-Tethyan OIB and a Jinshuikou Granite. The Sr and Nd isotopes and elemental concentrations for the Paleo-Tethyan OIB are from the Permian OIB-type alkaline basalts in the Zhiduo and Zaduo areas of the Tethyan domain (Average composition: I_{Sr} = 0.703627, $\varepsilon_{Nd(t)}$ = 4.5, Sr = 658.3 ppm, Nd = 39.6 ppm) (Ma et al., 2007). The data of the Jinshuikou granite are from a cordierite granite pluton at the northeastern margin of the Greater Tibetan plateau which is derived from partial melting of metagreywacke in the upper continental crust (Average composition: I_{Sr} = 0.737417, $\varepsilon_{Nd(t)}$ = -11.7, Sr = 196.2 ppm, Nd = 29.4 ppm) (Ba et al., 2012). ($K = (Sr/Nd)_{OIB} / (Sr/Nd)_{Granite}$, K_{max} and K_{min} represent the maximum and minimum values, $K_{average}$ denotes the ratio from average Sr and Nd concentrations of OIB and granite respectively).

Fig. 1

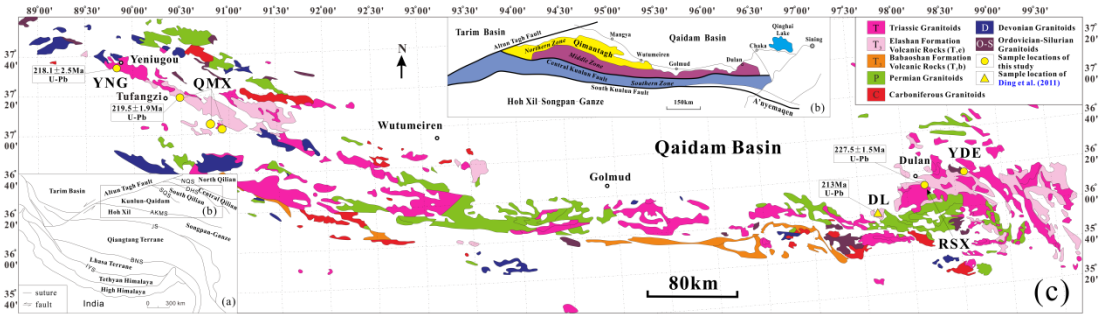

Fig. 2

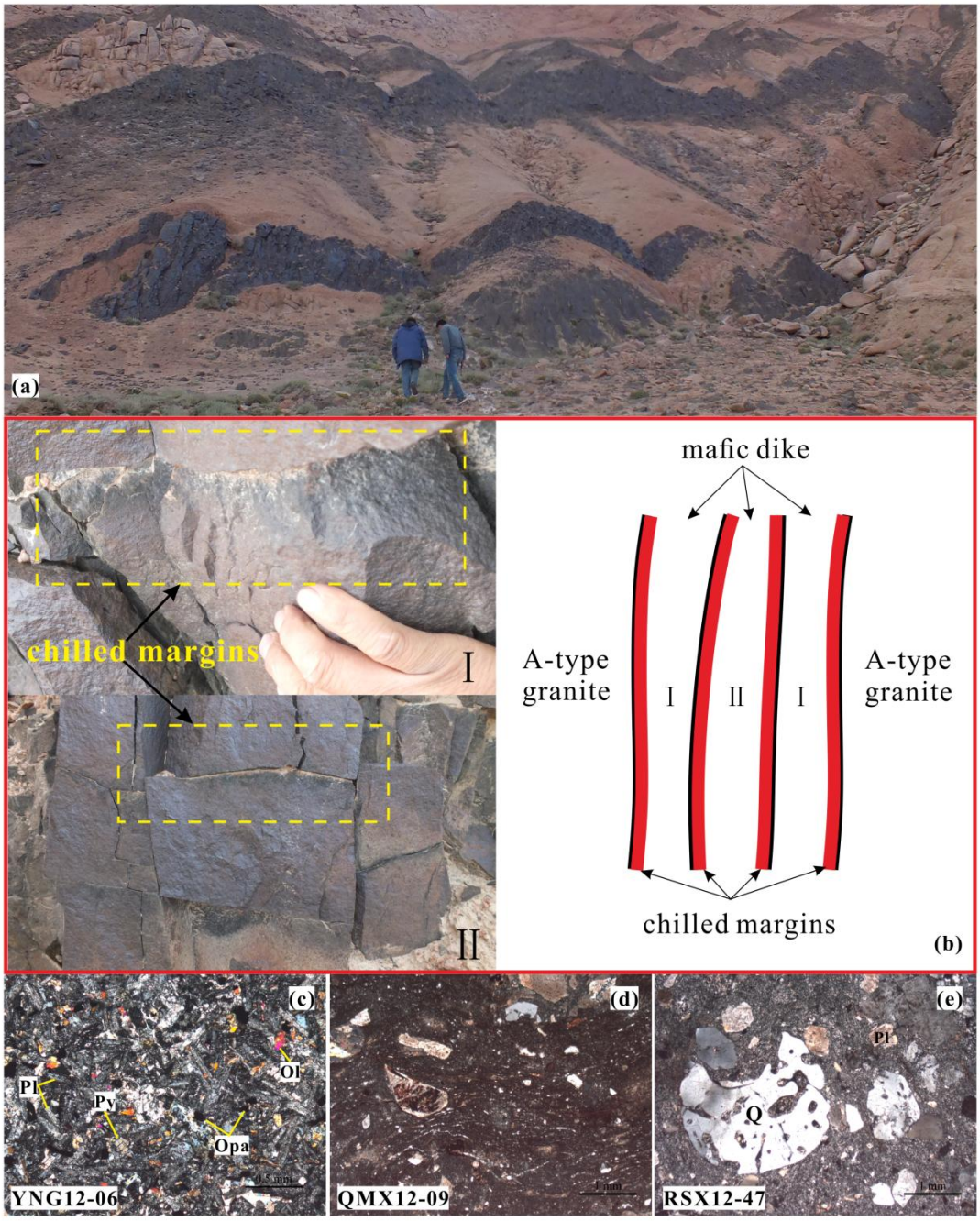

Fig. 3

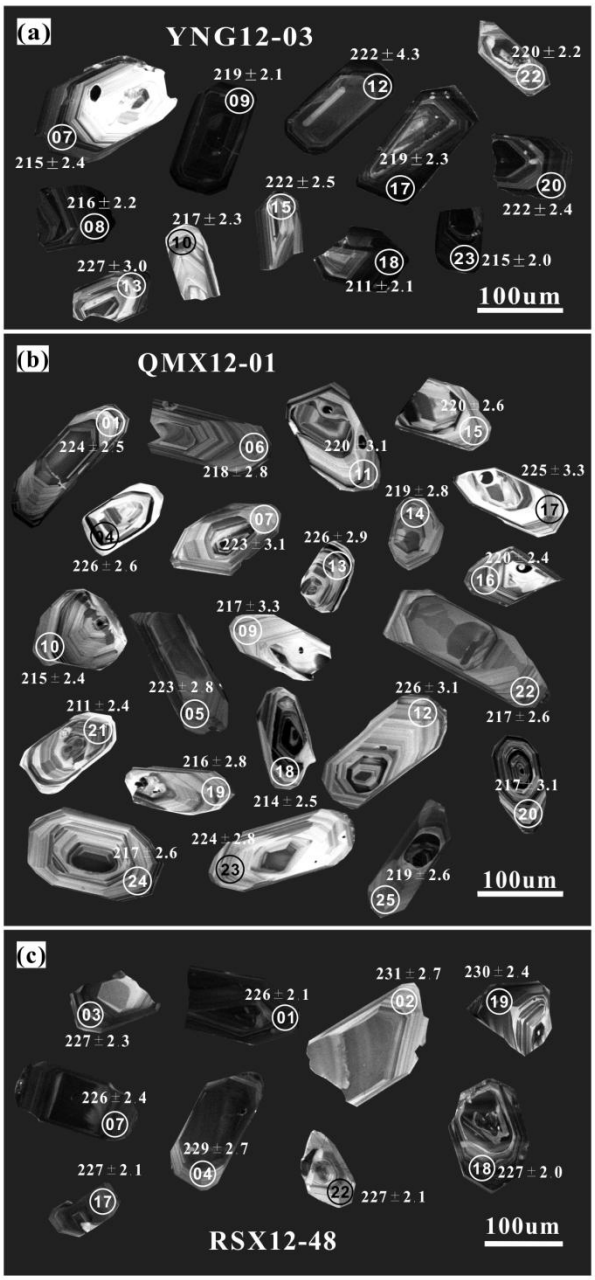

Fig. 4

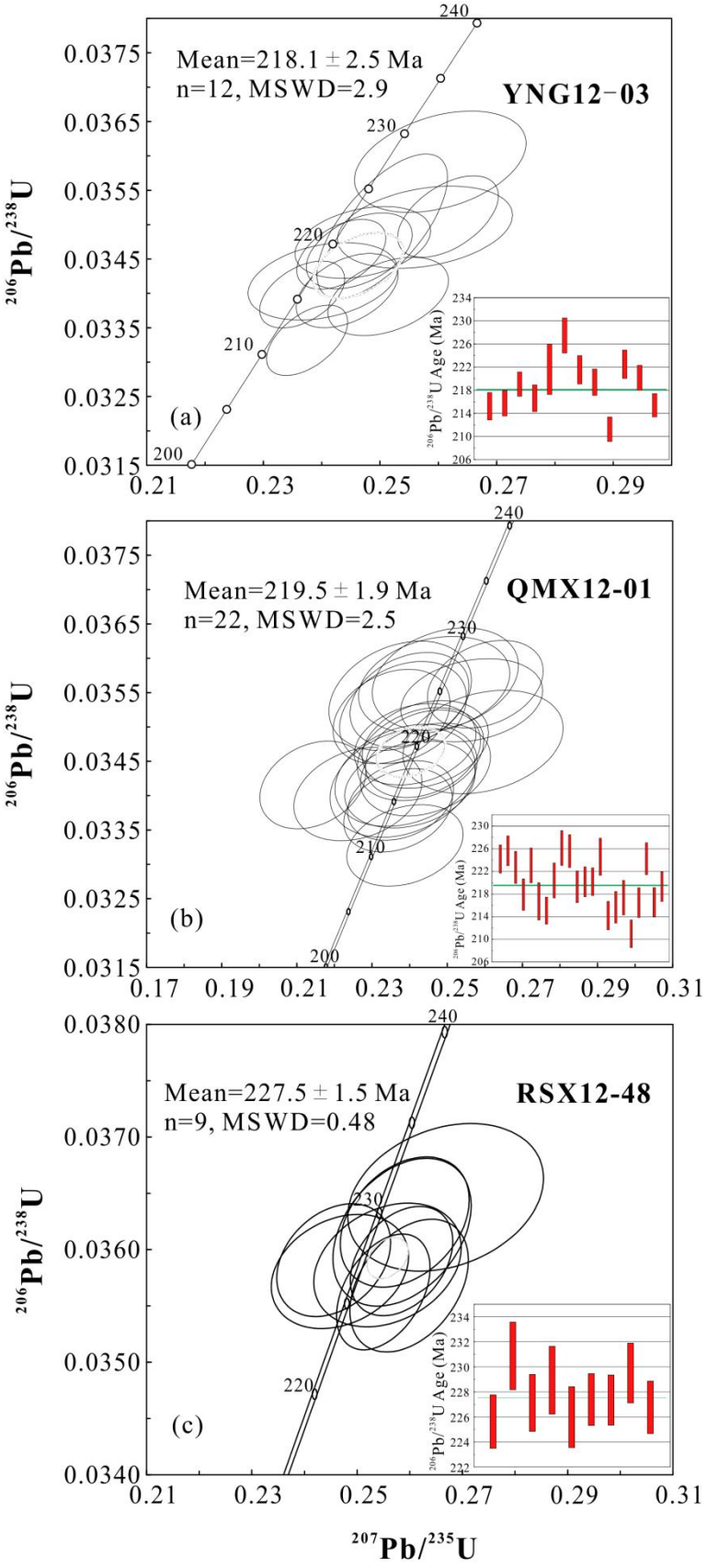

Fig. 5

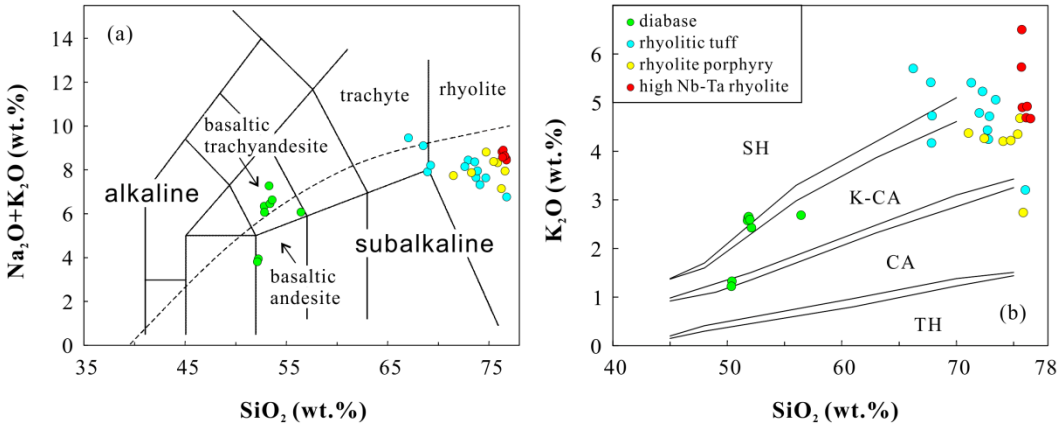

Fig. 6

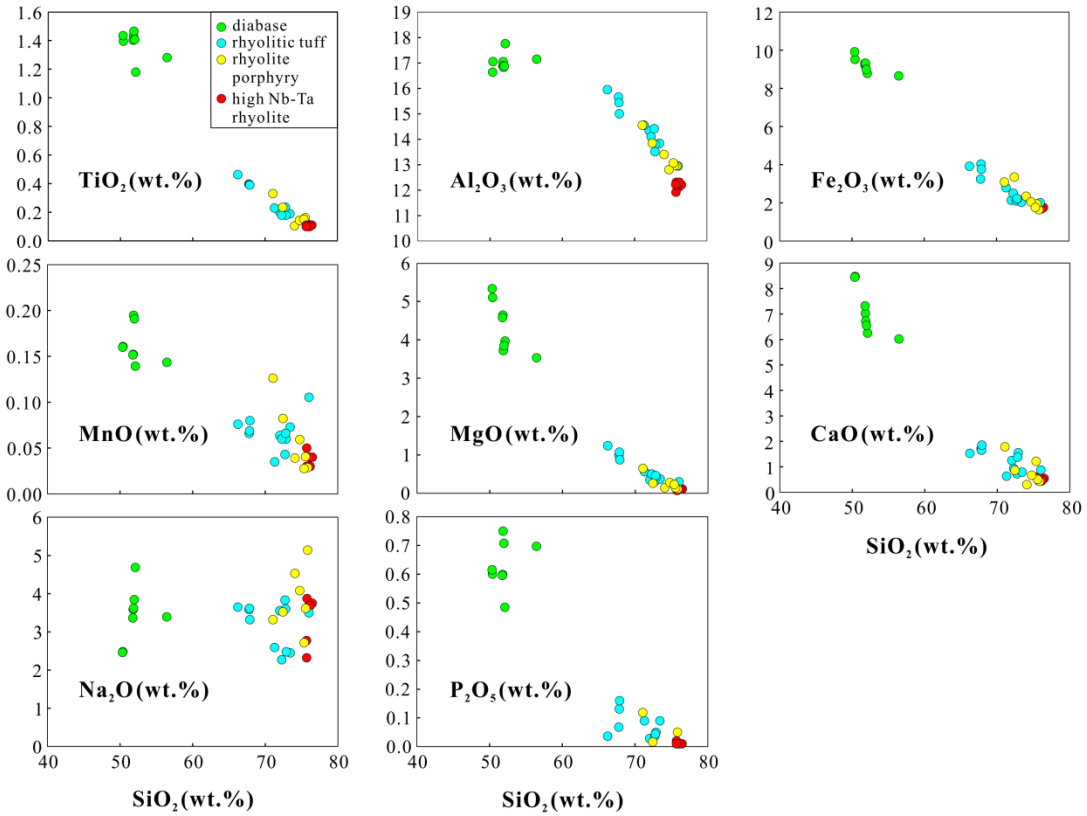

Fig. 7

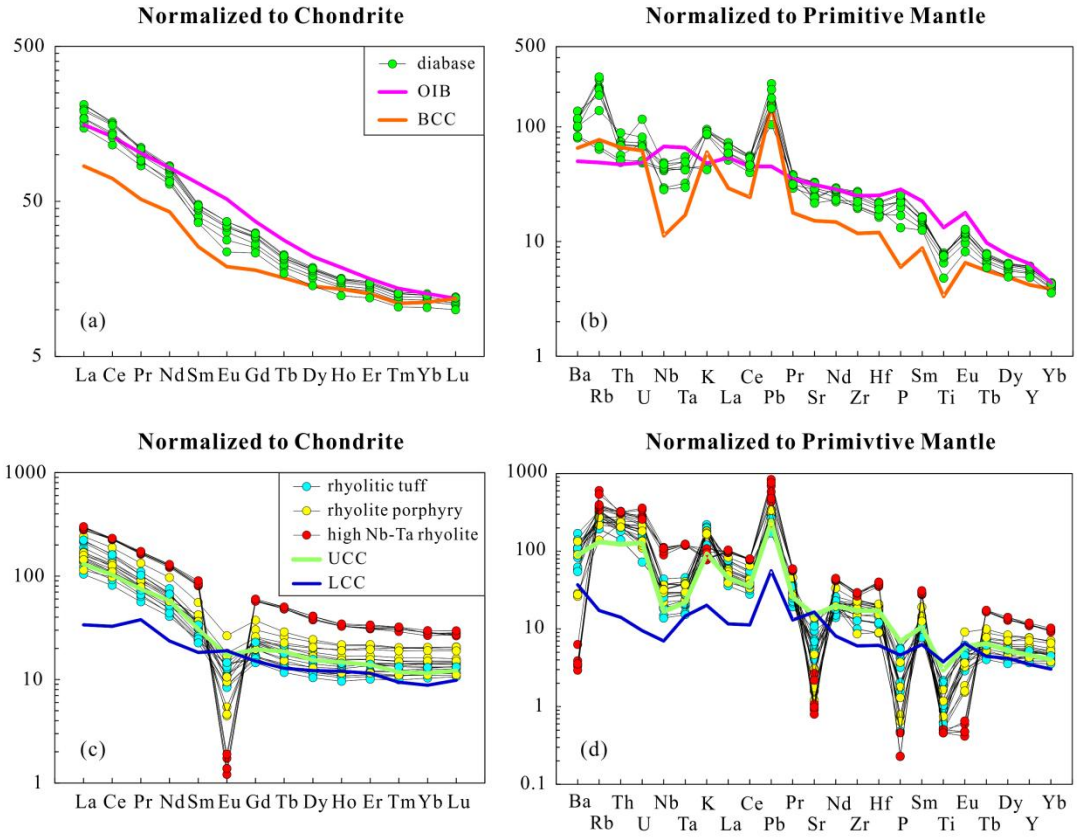

Fig. 8

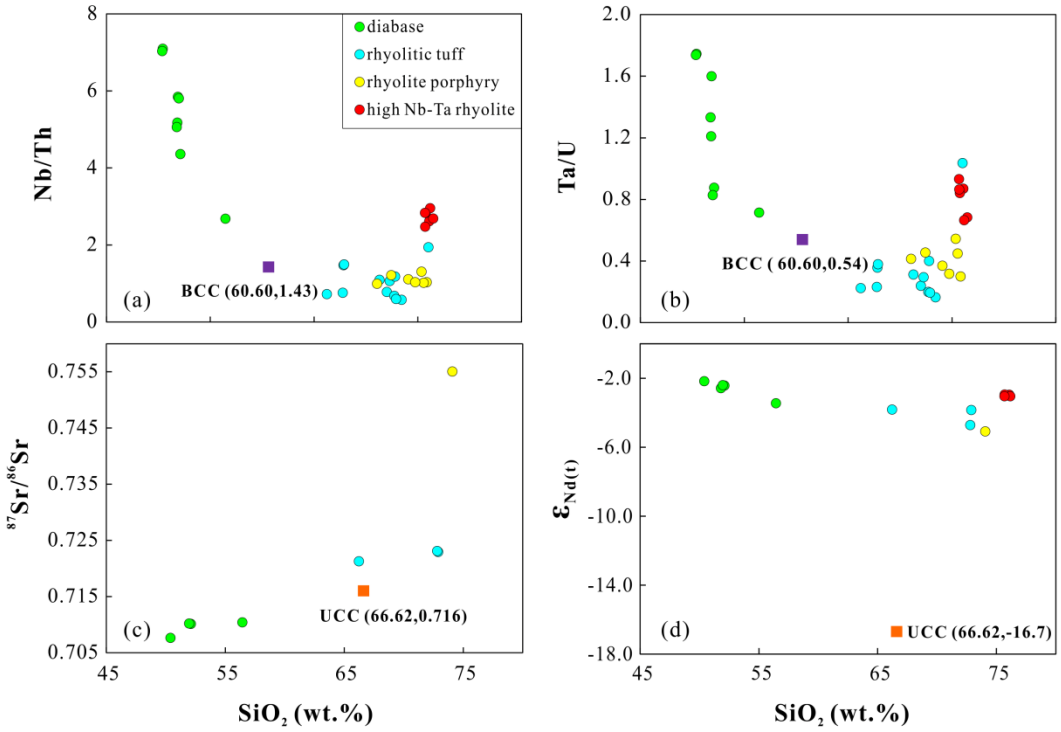

Fig. 9

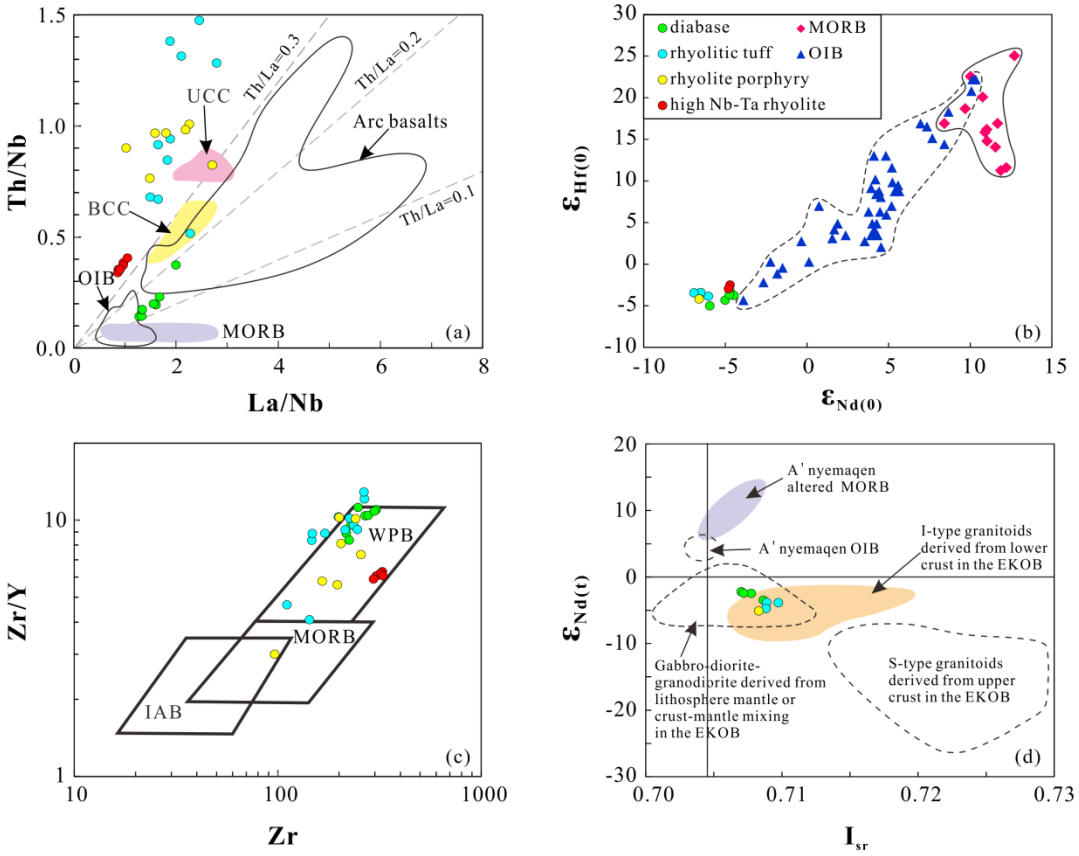

Fig. 10

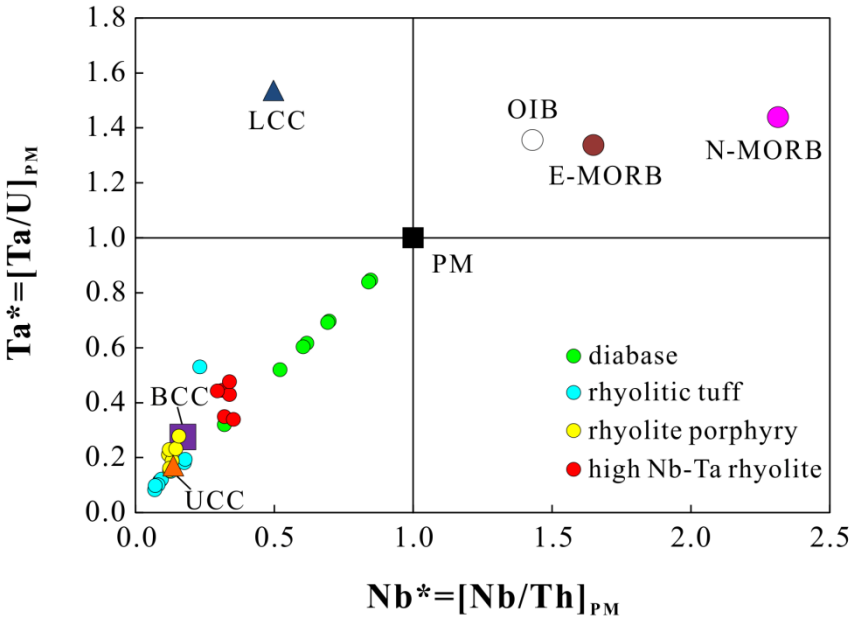

Fig. 11

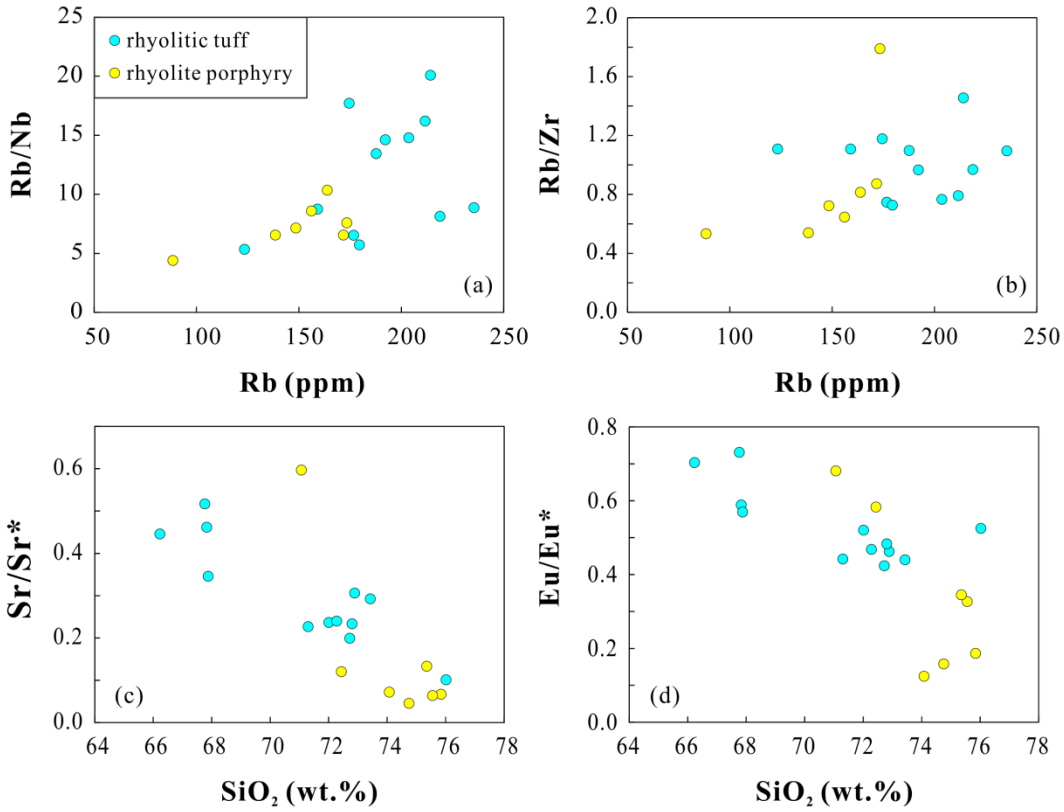

Fig. 12

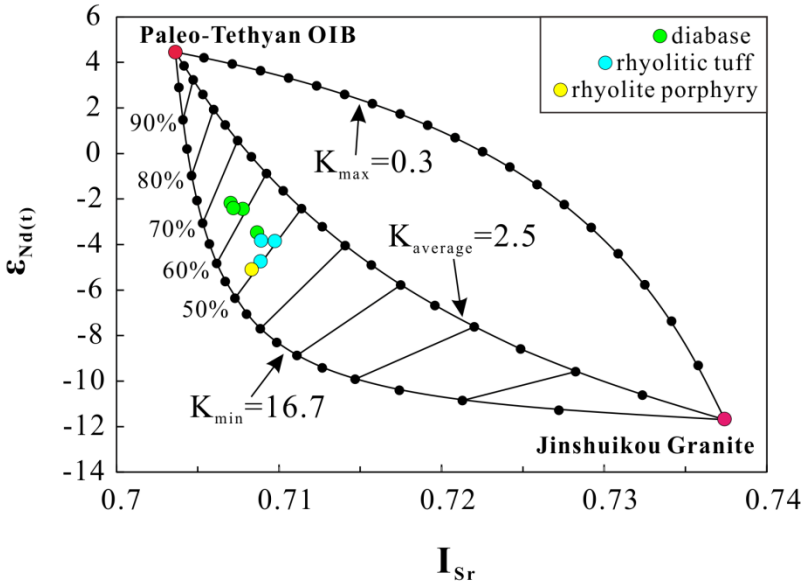

Table 1

Sample locations and zircon U-Pb ages of the late Triassic mafic dikes and felsic volcanic rocks in the East Kunlun Orogenic Belt.

Sample	GPS	Rock name	Age
YNG12-01	N37°34'30.3", E89°47'7.1"	diabase	
YNG12-03	N37°34'30.3", E89°47'7.1"	diabase	218.1±2.5 Ma
YNG12-04	N37°34'30.3", E89°47'7.1"	diabase	
YNG12-05	N37°34'30.3", E89°47'7.1"	diabase	
YNG12-06	N37°34'30.3", E89°47'7.1"	diabase	
YNG12-07	N37°34'30.3", E89°47'7.1"	diabase	
YNG12-08	N37°34'30.3", E89°47'7.1"	diabase	
QMX12-01	N37°18'34.8", E90°29'14.8"	rhyolitic tuff	219.5±1.9 Ma
QMX12-02	N37°18'34.9", E90°29'10.9"	rhyolitic tuff	
QMX12-03	N37°18'34.9", E90°29'9.0"	rhyolitic tuff	
QMX12-06	N37°18'42.1", E90°29'8.8"	rhyolitic tuff	
QMX12-07	N37°05'58.1", E90°47'58.3"	rhyolitic tuff	
QMX12-08	N37°05'58.1", E90°47'58.3"	rhyolitic tuff	
QMX12-09	N37°00'33.5", E90°56'23.8"	rhyolitic tuff	
QMX12-11	N37°00'33.5", E90°56'23.8"	diabase	
QMX12-10	N37°00'33.5", E90°56'23.8"	rhyolitic tuff	
QMX12-12	N37°00'33.5", E90°56'23.8"	rhyolitic tuff	
QMX12-13	N37°00'33.5", E90°56'23.8"	rhyolitic tuff	
RSX12-46	N36°10'55.9", E98°17'54.9"	rhyolite porphyry	
RSX12-47	N36°10'54.4", E98°17'53.4"	rhyolite porphyry	
RSX12-48	N36°10'46.7", E98°17'51.1"	rhyolite porphyry	227.5±1.5 Ma
RSX12-50	N36°10'46.7", E98°17'51.1"	rhyolite porphyry	
RSX12-51	N36°11'30.5", E98°13'58.9"	rhyolite porphyry	
YDE12-01	N36°18'45.4", E98°35'15.6"	rhyolitic tuff	
YDE12-02	N36°18'16.7", E98°36'40.5"	rhyolitic tuff	
YDE12-03	N36°17'13.2", E98°36'3.2"	rhyolite porphyry	
YDE12-16	N36°13'13.8", E98°42'21.92"	rhyolite porphyry	
DL09-01*	N36°00'38.64", E97°41'19.62"	high Nb-Ta rhyolite	214±1 Ma
DL09-02*	N36°00'38.64", E97°41'19.62"	high Nb-Ta rhyolite	
DL09-03*	N36°00'38.64", E97°41'19.62"	high Nb-Ta rhyolite	
DL09-04*	N36°00'38.64", E97°41'19.62"	high Nb-Ta rhyolite	
DL09-05*	N36°00'38.64", E97°41'19.62"	high Nb-Ta rhyolite	212±2 Ma
DL09-06*	N36°00'38.64", E97°41'19.62"	high Nb-Ta rhyolite	

* Data of high Nb-Ta rhyolite come from Ding et al. (2011).

Table 2

Zircon LA-ICP-MS U-Pb data of the late Triassic mafic dikes and felsic volcanic rocks from the East Kunlun Orogenic Belt.

Analysis	Pb	Th	U	Th/	Isotopic ratios						Apparent age (Ma)					
spot	(ppm)	(ppm)	(ppm)	U	207Pb/206Pb	1σ	207Pb/235U	1σ	206Pb/238U	1σ	207Pb/206Pb	1σ	207Pb/235U	1σ	206Pb/238U	1σ
YNG12-03 diabase, average age: 218.1±2.5 Ma, MSWD=2.9, n=12																
01	92	331	1013	0.33	0.0504	0.0017	0.2507	0.0082	0.0361	0.0004	213	78	227	7	229	3
02	212	808	2197	0.37	0.0509	0.0015	0.2742	0.0090	0.0390	0.0006	235	67	246	7	247	4
03	92	242	865	0.28	0.0639	0.0024	0.3237	0.0126	0.0368	0.0004	739	81	285	10	233	3
04	203	729	2290	0.32	0.0507	0.0014	0.2636	0.0072	0.0377	0.0004	233	61	238	6	239	3
05	199	795	2107	0.38	0.0512	0.0013	0.2539	0.0065	0.0360	0.0004	250	59	230	5	228	2
06	239	910	2533	0.36	0.0513	0.0015	0.2628	0.0077	0.0370	0.0004	254	65	237	6	234	2
07	335	1377	3767	0.37	0.0534	0.0013	0.2514	0.0068	0.0340	0.0004	346	56	228	6	215	2
08	350	1255	4979	0.25	0.0518	0.0011	0.2444	0.0058	0.0340	0.0004	276	45	222	5	216	2
09	490	1885	5893	0.32	0.0509	0.0010	0.2434	0.0050	0.0346	0.0003	235	44	221	4	219	2
10	123	555	994	0.56	0.0512	0.0019	0.2402	0.0085	0.0342	0.0004	256	85	219	7	217	2
11	312	700	2549	0.27	0.0572	0.0013	0.5127	0.0126	0.0648	0.0007	498	45	420	8	405	4
12	334	1356	3405	0.40	0.0523	0.0017	0.2504	0.0074	0.0350	0.0007	298	76	227	6	222	4
13	146	551	139	0.4	0.0528	0.00	0.2603	0.00	0.0359	0.00	320	11	235	8	227	3

			3	0		20		97		05		8				
14	346	1182	4117	0.29	0.0525	0.0013	0.3008	0.0076	0.0414	0.0005	306	56	267	6	261	3
15	123	503	1008	0.50	0.0535	0.0020	0.2577	0.0099	0.0350	0.0004	350	87	233	8	222	2
16	362	1214	3681	0.33	0.0520	0.0011	0.2843	0.0068	0.0394	0.0004	287	55	254	5	249	2
17	325	1333	3486	0.38	0.0514	0.0012	0.2464	0.0060	0.0346	0.0004	261	58	224	5	219	2
18	636	2508	7565	0.33	0.0515	0.0009	0.2375	0.0046	0.0333	0.0003	261	41	216	4	211	2
19	291	1082	3525	0.31	0.0521	0.0012	0.2633	0.0062	0.0365	0.0004	287	52	237	5	231	3
20	611	2188	6882	0.32	0.0537	0.0010	0.2617	0.0057	0.0351	0.0004	367	72	236	5	222	2
21	110	394	924	0.43	0.0532	0.0019	0.2898	0.0103	0.0395	0.0004	339	80	258	8	250	3
22	157	644	1549	0.42	0.0513	0.0016	0.2470	0.0077	0.0347	0.0003	254	70	224	6	220	2
23	425	1676	5121	0.33	0.0503	0.0010	0.2367	0.0048	0.0340	0.0003	209	46	216	4	215	2
24	167	438	658	0.67	0.0527	0.0018	0.4338	0.0154	0.0596	0.0007	322	78	366	11	373	4
QMX12-01 rhyolitic tuff, average age: 219.5±1.9 Ma, MSWD=2.5, n=22																
01	86	352	632	0.56	0.0530	0.0027	0.2565	0.0125	0.0354	0.0004	332	113	232	10	224	2
02	70	293	600	0.49	0.0612	0.0030	0.2744	0.0126	0.0331	0.0005	656	104	246	10	210	3
03	76	304	595	0.51	0.0586	0.0024	0.2783	0.0113	0.0346	0.0004	554	89	249	9	219	3
04	93	378	759	0.50	0.0531	0.0021	0.2601	0.0102	0.0356	0.0004	345	95	235	8	226	3
05	58	244	518	0.4	0.0489	0.00	0.2352	0.01	0.0352	0.00	143	10	214	8	223	3

				7		21		03		05		0			
06	65	285	595	0.48	0.0522	0.0026	0.2442	0.0114	0.0344	0.0004	295	139	222	9	218	3
07	63	275	516	0.53	0.0493	0.0024	0.2382	0.0111	0.0352	0.0005	165	117	217	9	223	3
08	66	232	472	0.49	0.0722	0.0037	0.3477	0.0179	0.0349	0.0005	991	104	303	13	221	3
09	42	185	406	0.45	0.0515	0.0029	0.2382	0.0128	0.0342	0.0005	261	131	217	10	217	3
10	89	414	749	0.55	0.0511	0.0020	0.2376	0.0093	0.0339	0.0004	256	97	216	8	215	2
11	53	218	448	0.49	0.0546	0.0030	0.2596	0.0141	0.0348	0.0005	398	92	234	11	220	3
12	46	186	410	0.45	0.0511	0.0028	0.2495	0.0128	0.0357	0.0005	243	130	226	10	226	3
13	100	448	679	0.66	0.0501	0.0026	0.2465	0.0133	0.0356	0.0005	211	122	224	11	226	3
14	57	252	508	0.50	0.0515	0.0024	0.2429	0.0111	0.0346	0.0004	265	107	221	9	219	3
15	65	285	494	0.58	0.0517	0.0025	0.2442	0.0111	0.0347	0.0004	333	118	222	9	220	3
16	103	453	787	0.57	0.0504	0.0022	0.2415	0.0107	0.0347	0.0004	213	106	220	9	220	2
17	64	259	497	0.52	0.0487	0.0026	0.2375	0.0125	0.0355	0.0005	200	124	216	10	225	3
18	131	580	1040	0.56	0.0511	0.0021	0.2369	0.0095	0.0338	0.0004	256	96	216	8	214	3
19	50	223	495	0.45	0.0486	0.0024	0.2262	0.0113	0.0340	0.0004	128	-81	207	9	216	3
20	62	286	548	0.52	0.0508	0.0027	0.2391	0.0125	0.0343	0.0005	232	124	218	10	217	3
21	80	342	777	0.44	0.0524	0.0022	0.2388	0.0102	0.0333	0.0004	302	92	217	8	211	2
22	53	236	513	0.46	0.0462	0.0021	0.2142	0.0093	0.0342	0.0004	9	113	197	8	217	3
23	57	245	514	0.48	0.0493	0.0022	0.2399	0.0105	0.0354	0.0005	167	106	218	9	224	3
24	59	260	510	0.51	0.0512	0.0025	0.2401	0.0115	0.0342	0.0004	250	83	218	9	217	3
25	67	290	628	0.46	0.0508	0.0021	0.2436	0.0101	0.0346	0.0004	232	96	221	8	219	3

RSX12-4

8, rhyolite porphyry, average age: 227.5±1.5 Ma, MSWD=0.48, n=9															
01	293	1220	2735	0.45	0.0518	0.0012	0.2550	0.0059	0.0356	0.0003	276	47	231	5	226	2
02	59	241	448	0.54	0.0531	0.0025	0.2668	0.0123	0.0365	0.0004	332	107	240	10	231	3
03	127	555	828	0.67	0.0521	0.0020	0.2558	0.0092	0.0359	0.0004	300	89	231	7	227	2
04	147	688	864	0.80	0.0523	0.0018	0.2585	0.0087	0.0362	0.0004	298	80	233	7	229	3
05	196	727	2116	0.34	0.0539	0.0015	0.2766	0.0086	0.0370	0.0005	369	63	248	7	234	3
06	143	627	900	0.70	0.0551	0.0020	0.2792	0.0101	0.0368	0.0004	413	83	250	8	233	3
07	181	742	1650	0.45	0.0526	0.0015	0.2599	0.0074	0.0357	0.0004	309	65	235	6	226	2
08	204	862	1331	0.65	0.0684	0.0025	0.3347	0.0121	0.0353	0.0004	880	-123	293	9	224	2
09	193	771	1651	0.47	0.0525	0.0013	0.2722	0.0067	0.0376	0.0004	306	55	244	5	238	2
10	62	214	275	0.78	0.0533	0.0031	0.3141	0.0172	0.0429	0.0006	343	133	277	13	271	4
11	118	430	647	0.66	0.0796	0.0055	0.4402	0.0364	0.0378	0.0005	1187	137	370	26	239	3
12	113	425	725	0.59	0.0663	0.0028	0.3582	0.0161	0.0389	0.0006	817	89	311	12	246	4
13	531	762	1838	0.41	0.1502	0.0037	0.8778	0.0199	0.0424	0.0004	2350	42	640	11	268	3
14	282	1194	2161	0.55	0.0542	0.0014	0.2771	0.0072	0.0369	0.0004	376	59	248	6	234	2
15	986	3615	7463	0.48	0.0670	0.0019	0.3344	0.0121	0.0353	0.0004	839	60	293	9	223	3
16	165	677	1237	0.55	0.0548	0.0017	0.2813	0.0088	0.0371	0.0003	467	73	252	7	235	2
17	229	107	155	0.6	0.0498	0.00	0.2456	0.00	0.0359	0.00	183	66	223	6	227	2

		1	3	9		15		71		03						
18	267	109 3	268 8	0.4 1	0.0522	0.00 13	0.2584	0.00 64	0.0359	0.00 03	295	57	233	5	227	2
19	192	860	135 2	0.6 4	0.0521	0.00 16	0.2591	0.00 81	0.0362	0.00 04	287	77	234	7	230	2
20	171	684	125 1	0.5 5	0.0597	0.00 22	0.2996	0.01 15	0.0362	0.00 03	591	81	266	9	229	2
21	142	617	768	0.8 0	0.0583	0.00 22	0.2996	0.01 16	0.0372	0.00 04	539	83	266	9	235	3
22	197	927	113 9	0.8 1	0.0501	0.00 17	0.2467	0.00 86	0.0358	0.00 03	198	77	224	7	227	2

Table 3

Whole-rock major and trace element data of the late Triassic mafic dikes and felsic volcanic rocks in the East Kunlun Orogenic Belt.

Sample	YNG12-01	YNG12-03	YNG12-04	YNG12-05	YNG12-06	YNG12-07	YNG12-08	QMX12-11	QMX12-01	QMX12-02	QMX12-03
	mafic (diabase)								*felsic (rhyolitic tuff)*		
Major element (wt.%)											
SiO2	52.11	50.40	50.35	51.82	51.76	51.86	51.97	56.44	66.23	67.76	72.01
TiO2	1.18	1.40	1.44	1.43	1.40	1.47	1.41	1.28	0.46	0.40	0.20
Al2O3	17.76	17.06	16.64	17.05	16.90	16.83	16.87	17.15	15.95	15.66	14.34
Fe2O3a	8.78	9.52	9.91	9.20	9.30	9.32	9.00	8.65	3.91	3.24	2.14
MnO	0.14	0.16	0.16	0.15	0.15	0.19	0.19	0.14	0.08	0.07	0.06
MgO	3.97	5.11	5.34	4.65	4.59	3.72	3.85	3.54	1.24	0.99	0.35
CaO	6.25	8.47	8.45	7.02	7.32	6.72	6.55	6.02	1.53	1.71	1.25
Na2O	4.68	2.48	2.46	3.58	3.36	3.62	3.84	3.39	3.65	3.58	3.55
K2O	2.43	1.33	1.22	2.64	2.58	2.66	2.59	2.69	5.70	5.42	4.79
P2O5	0.48	0.60	0.62	0.60	0.60	0.75	0.71	0.70	0.04	0.07	0.03
LOI b	1.49	3.13	2.96	1.64	1.53	2.72	2.74	2.13	0.63	0.79	0.64
Total	99.27	99.65	99.54	99.78	99.49	99.86	99.72	102.13	99.42	99.70	99.36
Mg# c	0.50	0.54	0.54	0.53	0.52	0.47	0.49	0.47	0.41	0.40	0.26
Trace element (ppm)											
Sc	21.6	21.3	22.5	22.3	21.9	20.0	19.6	13.0	6.07	5.33	3.23
V	178	169	186	168	168	155	147	96.7	29.2	32.3	8.55
Cr	51.0	95.0	94.1	84.5	80.7	68.2	65.1	30.2	4.85	5.94	3.06
Co	21.7	26.2	26.3	22.6	23.3	21.2	21.0	14.9	5.46	5.09	1.25
Ni	14.5	42.8	42.5	29.3	33.6	28.3	26.5	14.0	2.01	2.81	0.73
Ga	19.1	17.5	18.1	18.4	18.6	18.5	18.0	17.6	17.2	18.3	15.4
Rb	140	40.4	42.7	135	119	163	172	88.0	212	204	188
Sr	531	599	611	695	681	492	513	456	155	199	112
Y	24.0	24.5	26.9	25.9	26.7	27.7	27.5	22.2	22.1	20.6	19.2
Zr	230	218	225	269	279	305	299	249	267	266	171

Nb	20.922	29.565	30.631	30.821	31.930	34.631	33.755	20.206	13.060	13.768	13.966
Cs	4.448	3.744	4.206	10.110	11.766	8.762	5.240	8.152	4.852	4.856	6.572
Ba	691.00	559.20	574.40	818.60	958.20	806.60	822.20	705.80	1184.40	977.40	580.80
Hf	5.345	5.040	5.270	6.138	6.398	6.826	6.661	5.900	6.252	6.149	4.407
Ta	1.322	1.774	1.840	1.728	2.026	2.250	2.026	1.216	0.806	0.849	0.966
Pb	10.766	11.254	7.424	16.858	11.014	14.966	12.620	10.262	21.480	20.380	21.560
Th	4.796	4.164	4.352	5.952	6.308	5.922	5.810	7.528	18.034	18.088	17.910
U	1.510	1.017	1.059	1.428	1.520	1.407	2.448	1.704	3.612	3.676	4.050
La	35.16	37.96	40.86	49.66	49.92	46.46	45.30	40.44	24.66	29.04	39.06
Ce	70.80	79.12	84.64	97.60	99.34	96.80	94.88	82.14	49.66	56.42	74.82
Pr	8.04	8.60	9.40	10.20	10.38	10.57	10.34	8.71	5.34	6.02	7.62
Nd	30.14	32.44	35.68	37.32	38.18	39.68	38.94	31.30	18.96	20.74	24.88
Sm	5.71	6.11	6.72	6.73	6.94	7.31	7.20	5.58	3.68	3.65	4.12
Eu	1.63	1.84	1.97	1.97	2.03	2.14	2.15	1.37	0.81	0.82	0.64
Gd	5.17	5.47	6.06	5.96	6.10	6.44	6.35	4.77	3.42	3.22	3.48
Tb	0.70	0.73	0.81	0.78	0.80	0.85	0.83	0.64	0.53	0.48	0.51
Dy	4.05	4.22	4.62	4.45	4.58	4.76	4.67	3.62	3.35	2.95	2.98
Ho	0.79	0.81	0.88	0.85	0.87	0.90	0.89	0.70	0.72	0.64	0.61
Er	2.19	2.27	2.47	2.36	2.41	2.51	2.46	1.97	2.25	2.01	1.85
Tm	0.29	0.30	0.32	0.31	0.32	0.33	0.33	0.27	0.35	0.31	0.28
Yb	1.91	1.96	2.11	2.05	2.11	2.16	2.11	1.76	2.39	2.18	1.93
Lu	0.27	0.28	0.30	0.29	0.30	0.31	0.30	0.25	0.36	0.34	0.29
(La/Yb)N d	13.22	13.90	13.89	17.41	16.99	15.44	15.40	16.50	7.41	9.56	14.53
Eu/Eu*e	0.92	0.97	0.95	0.95	0.95	0.96	0.97	0.81	0.70	0.73	0.52
Sr/Sr*e	0.99	1.04	0.97	1.03	0.99	0.70	0.74	0.80	0.45	0.52	0.24

Table 3 (continued)

Sample	QMX12-06	QMX12-07	QMX12-08	QMX12-09	QMX12-10	QMX12-12	QMX12-13	YDE12-01	YDE12-02	RSX12-46	RSX12-47
	felsic (rhyolitic tuff)									*felsic (rhyolite porphyry)*	

Major element (wt.%)											
SiO2	72.72	73.43	72.89	71.30	67.83	72.28	67.88	76.02	72.80	71.07	75.84
TiO2	0.21	0.19	0.18	0.23	0.39	0.18	0.39	0.11	0.24	0.33	0.11
Al2O3	14.42	13.84	13.80	14.56	15.44	14.10	15.01	12.94	13.51	14.56	12.95
Fe2O3 a	2.09	2.03	2.20	2.79	4.03	2.50	3.76	2. 0	2.22	3.09	1.64
MnO	0.04	0.07	0.06	0.04	0.07	0.06	0.08	0.11	0.07	0.13	0.03
MgO	0.31	0.37	0.42	0.56	1.07	0.50	0.87	0.30	0.46	0.65	0.11
CaO	0.72	0.79	1.55	0.63	1.65	0.93	1.85	0.87	1.38	1.78	0.43
Na2O	3.83	2.45	2.48	2.59	3.62	2.27	3.32	3.50	3.60	3.32	5.14
K2O	4.44	5.06	4.72	5.41	4.17	5.23	4.73	3.21	4.25	4.37	2.74
P2O5	0.04	0.09	0.05	0.09	0.13	<0.03	0.16	<0.03	0.04	0.12	0.05
LOI b	0.57	0.77	0.71	0.87	1.22	0.87	1.11	0.62	0.67	0.40	0.19
Total	99.40	99.09	99.06	99.06	99.62	98.92	99.16	99.68	99.24	99.81	99.23
Mg# c	0.25	0.29	0.30	0.31	0.37	0.31	0.34	0.25	0.31	0.32	0.13
Trace element (ppm)											
Sc	2.95	3.13	3.03	3.61	6.66	3.63	6.84	4.44	5.07	5.52	4.67
V	6.75	12.1	11.6	10.2	37.8	9.99	30.8	4.02	9.08	26.5	3.40
Cr	4.93	3.82	7.37	7.68	14.3	5.67	14.1	2.67	3.82	6.31	3.55
Co	1.04	1.62	1.74	1.89	5.06	1.60	4.66	0.69	1.32	2.90	0.17
Ni	1.76	1.86	3.57	3.47	6.42	2.36	5.83	1.94	1.25	3.11	0.71
Ga	15.7	15.7	14.6	17.4	17.3	17.1	18.9	15.8	16.0	18.1	16.9
Rb	192	214	175	219	177	235	179	123	159	164	88.5
Sr	85.5	126	120	124	244	146	229	60.9	105	295	33.3
Y	19.3	17.6	16.7	22.2	24.8	23.4	26.8	23.8	35.1	19.6	28.7
Zr	199	147	148	226	236	215	247	111	144	201	166
Nb	13.140	10.667	9.851	26.910	27.018	26.514	31.392	23.100	18.180	15.824	20.106
Cs	4.984	3.988	3.644	5.188	5.468	5.674	4.224	3.830	6.830	4.568	1.851
Ba	406.80	436.80	383.00	778.80	758.60	699.80	765.60	761.20	766.20	775.40	200.00
Hf	4.794	3.708	3.552	5.480	5.819	5.334	6.191	2.738	3.702	5.080	4.740
Ta	0.868	0.664	0.628	1.491	1.652	1.545	1.878	1.582	1.146	0.960	1.178
Pb	21.620	19.482	15.924	16.254	23.660	15.846	21.060	12.220	18.922	32.320	13.876
Th	19.374	18.540	16.540	24.600	18.338	24.940	20.980	11.886	15.366	15.928	19.442

U	4.358	4.048	3.238	4.786	4.642	5.248	4.954	1.528	2.862	2.318	3.928
La	32.34	35.80	32.46	44.50	40.50	50.18	51.92	52.70	33.36	35.82	32.08
Ce	63.90	66.86	61.70	83.82	77.70	93.92	99.58	98.44	65.28	71.38	66.78
Pr	6.78	6.90	6.28	8.77	8.28	9.72	10.45	9.68	6.95	7.67	7.59
Nd	22.74	22.38	20.50	28.78	28.40	31.78	35.22	31.22	24.24	26.74	27.26
Sm	3.97	3.78	3.45	4.81	5.05	5.25	6.02	5.17	4.85	4.74	5.41
Eu	0.51	0.50	0.48	0.63	0.92	0.73	1.04	0.85	0.77	0.97	0.31
Gd	3.38	3.26	2.99	3.99	4.52	4.38	5.19	4.70	4.87	4.03	4.89
Tb	0.50	0.48	0.44	0.60	0.68	0.64	0.77	0.67	0.80	0.57	0.76
Dy	3.07	2.86	2.64	3.58	4.02	3.79	4.42	3.97	5.10	3.28	4.67
Ho	0.64	0.59	0.54	0.75	0.82	0.78	0.89	0.81	1.10	0.65	0.95
Er	1.95	1.76	1.67	2.34	2.40	2.35	2.59	2.33	3.34	1.91	2.80
Tm	0.30	0.28	0.25	0.36	0.36	0.36	0.38	0.34	0.51	0.28	0.41
Yb	2.11	1.91	1.75	2.47	2.39	2.46	2.56	2.22	3.44	1.87	2.75
Lu	0.32	0.29	0.27	0.37	0.36	0.37	0.38	0.34	0.52	0.28	0.40
(La/Yb) N d	10.99	13.48	13.28	12.90	12.17	14.63	14.56	17. 0	6.95	13.74	8.36
Eu/Eu* e	0.42	0.44	0.46	0.44	0.59	0.47	0.57	0.52	0.48	0.68	0.19
Sr/Sr* e	0.20	0.29	0.31	0.23	0.46	0.24	0.35	0.10	0.23	0.60	0.07

Table 3 (continued)

Sample	RSX12-48	RSX12-50	RSX12-51	YDE12-03	YDE12-16	DL09-01	DL09-02	DL09-03	DL09-04	DL09-05	DL09-06
	felsic (rhyolite porphyry)					*felsic (high Nb-Ta rhyolite)*					
Major element (wt.%)											
SiO2	74.08	75.56	74.75	72.44	75.36	76.10	75.76	75.71	76.48	76.18	75.69
TiO2	0.11	0.16	0.14	0.24	0.15	0.10	0.10	0.11	0.11	0.10	0.10
Al2O3	13.40	12.97	12.81	13.85	13.07	12.12	12.31	11.92	12.21	12.31	12.22
Fe2O3	2.34	1.93	2.05	3.35	1.75	1.81	1.82	1.83	1.76	1.68	1.82

a											
MnO	0.04	0.04	0.06	0.08	0.03	0.04	0.03	0.05	0.04	0.03	0.03
MgO	0.14	0.14	0.28	0.26	0.23	0.14	0.07	0.12	0.11	0.10	0.16
CaO	0.30	0.50	0.67	0.86	1.21	0.44	0.44	0.51	0.54	0.49	0.61
Na2O	4.53	3.62	4.08	3.52	2.72	3.75	3.87	2.32	3.75	3.68	2.77
K2O	4.21	4.68	4.22	4.26	4.35	4.69	4.90	6.50	4.67	4.92	5.73
P2O5	<0.03	<0.03	<0.03	0.02	<0.03	0.01	0.01	0.02	0.01	0.01	0.01
LOI b	0.14	0.22	0.26	0.43	0.72	0.76	0.60	0.94	0.39	0.45	0.71
Total	99.28	99.82	99.32	99.30	99.58	99.96	99.91	100.03	100.07	99.95	99.85
Mg# c	0.12	0.14	0.23	0.15	0.22	0.15	0.08	0.13	0.12	0.12	0.16
Trace element (ppm)											
Sc	5.07	5.19	4.79	11.2	5.07	2.97	2.57	3.32	2.67	2.96	3.07
V	6.67	3.99	6.01	10.5	6.75						
Cr	3.56	2.54	5.81	3.96	3.30	1.97	2.50	2.40	1.85	1.60	1.71
Co	0.47	0.29	0.47	1.54	0.97	0.57	0.54	0.76	0.64	0.55	0.62
Ni	0.93	0.72	2.69	1.23	0.77	1.59	1.66	2.24	1.77	1.31	1.69
Ga	20.5	17.3	16.9	17.0	15.6						
Rb	172	156	148	138	173	215	246	384	241	253	342
Sr	34.5	36.8	25.5	99.3	64.7	19.3	16.9	56.5	22.8	20.8	46.3
Y	35.1	23.9	25.3	35.0	32.3	51.5	50.4	50.2	51.9	52.0	54.2
Zr	197	242	205	257	97	318	306	296	327	323	329
Nb	26.208	18.162	20.772	21.112	22.824	72.700	75.400	63.800	71.500	80.100	78.000
Cs	3.686	1.111	2.342	4.678	6.764						
Ba	184.62	708.40	193.42	936.34	628.60	24.80	23.20	44.00	27.20	20.60	24.80
Hf	6.042	5.880	5.630	6.457	2.788	12.300	12.000	10.900	11.400	11.600	12.400
Ta	1.665	1.119	1.209	1.214	1.538	4.900	5.060	4.860	4.900	5.020	5.040
Pb	22.480	16.460	24.240	16.562	24.000	59.700	49.200	41.500	31.100	34.200	54.100
Th	23.580	17.830	20.100	17.380	17.418	27.800	26.600	25.800	26.600	27.100	27.500
U	4.508	2.494	3.814	2.668	2.826	5.640	6.020	5.620	7.170	7.560	5.410
La	27.00	39.80	37.54	57.33	34.06	70.70	66.00	67.30	69.50	69.30	71.10
Ce	59.56	80.76	77.32	115.20	67.46	137.00	138.00	139.00	140.00	141.00	142.00
Pr	7.13	8.87	8.56	12.64	7.43	16.30	15.40	15.70	15.80	15.90	16.40
Nd	27.04	31.14	30.38	45.16	26.54	60.00	56.40	58.10	58.40	58.80	60.60
Sm	6.45	5.57	5.56	8.50	5.57	13.20	12.30	12.40	12.80	12.80	13.80
Eu	0.26	0.55	0.27	1.54	0.61	0.08	0.07	0.10	0.08	0.08	0.11

Gd	6.21	4.74	4.82	7.66	5.31	12.30	11.80	11.90	12.00	11.70	12.30
Tb	0.97	0.69	0.71	1.08	0.84	1.87	1.85	1.79	1.80	1.80	1.88
Dy	5.85	4.05	4.24	6.17	5.19	10.40	9.82	9.79	9.54	9.82	10.40
Ho	1.20	0.81	0.87	1.23	1.08	1.90	1.86	1.85	1.85	1.85	1.95
Er	3.50	2.36	2.58	3.59	3.23	5.46	5.18	5.10	5.11	5.24	5.58
Tm	0.51	0.34	0.38	0.52	0.48	0.81	0.78	0.78	0.74	0.81	0.82
Yb	3.39	2.25	2.56	3.47	3.23	4.74	4.84	4.81	4.51	4.76	5.05
Lu	0.50	0.34	0.38	0.52	0.48	0.72	0.70	0.67	0.69	0.69	0.75
(La/Yb)N d	5.71	12.70	10.51	11.84	7.55	6.58	6.91	7.18	6.54	6.90	6.73
Eu/Eu*e	0.12	0.33	0.16	0.58	0.35	0.02	0.02	0.03	0.02	0.02	0.03
Sr/Sr* e	0.07	0.06	0.05	0.12	0.13	0.02	0.02	0.05	0.02	0.02	0.04

a. Fe2O3 is total Fe expressed as Fe3+.

b. LOI (Loss On Ignition) is conformed to the equation: LOI = (Mbefore — Mafter) / Mbefore × 100% in which Mafter represents for the mass reweighed after heating at 1000°C in the furnace for several hours and Mbefore is the initial mass about 0.5g.

c. Mg# = molar Mg/[Mg+Fe2+] with 10% total Fe as Fe3+.

d. Subscript N stands for normalised values against Chondrite.

e. Eu/Eu* = EuPM/[SmPM*GdPM]1/2, Sr/Sr* = SrPM/[PrPM*NdPM]1/2, where subscript PM denotes normalised values against Primary Mantle.

Table 4

Whole rock Sr-Nd isotopic composition of the late Triassic mafic dikes and felsic volcanic rocks from the East Kunlun Orogenic Belt.

Sample	Rb (ppm)	Sr (ppm)	87Rb/86Sr	87Sr/86Sr	±2σ	Isr	Sm (ppm)	Nd (ppm)	147Sm/144Nd	143Nd/144Nd	±2σ	143Nd/144Ndi	εNd(t)	t (Ma)
YNG12-01	140.3	531.4	0.76	0.710137	10	0.707766	5.71	30.14	0.1154	0.512397	5	0.512232	-2.44	218
YNG12-03	40.4	599.2	0.20	0.707622	4	0.707017	6.11	32.44	0.1147	0.512409	8	0.512246	-2.18	218
YNG12-05	134.7	694.6	0.56	—	—	—	6.73	37.32	0.1098	0.512381	3	0.512225	-2.59	218
YNG12-08	172.3	512.8	0.97	0.710202	16	0.707185	7.20	38.94	0.1126	0.512395	6	0.512234	-2.40	218
QMX12-11	88.0	456.4	0.56	0.710396	4	0.708649	5.58	31.30	0.1084	0.512333	2	0.512177	-3.46	220
QMX12-01	211.6	154.9	3.96	0.721267	4	0.708892	3.68	18.96	0.1180	0.512329	4	0.512159	-3.83	220
QMX12-08	174.5	119.9	4.21	0.722926	5	0.709741	3.45	20.50	0.1023	0.512305	3	0.512157	-3.85	220
YDE12-02	159.1	104.7	4.40	0.723118	5	0.708852	4.85	24.24	0.1217	0.512284	5	0.512102	-4.73	228
RSX12-48	171.7	34.5	14.41	0.755049	4	0.708316	6.45	27.04	0.1452	0.512300	4	0.512083	-5.09	228
DL09-01*	215.0	19.3	32.53	0.834890	9	0.736354	13.20	60.00	0.1330	0.512397	5	0.512212	-2.97	213
DL09-03*	384.0	56.5	19.78	0.764700	8	0.704799	12.40	58.10	0.1290	0.512392	4	0.512212	-2.96	213
DL09-05*	253.0	20.8	35.54	0.841700	9	0.734031	12.80	58.80	0.1316	0.512391	10	0.512208	-3.05	213
DL09-06*	342.0	46.3	21.44	0.772000	4	0.707064	13.80	60.60	0.1377	0.512399	4	0.512207	-3.06	213

Isr=[(87Sr/86Sr)-(87Rb/86Sr)(eλt-1)]; 143Nd/144Ndi=[(143Nd/144Nd)-(147Sm/144Nd)(eλt-1)];
εNd(t)=[(143Nd/144Ndi)/(143Nd/144NdCHURi)-1]×104.
147Sm/144NdCHUR=0.1967; 143Nd/144NdCHUR=0.512638; λ(87Rb)=1.42×10-11yr-1;
λ(147Sm)=6.54×10-12yr-1.

— Not detected.

*Data come from Ding et al. (2011).

Table 5

Whole rock Hf isotopic composition of the late Triassic mafic dikes and felsic volcanic rocks from the East Kunlun Orogenic Belt.

Sample	Lu (ppm)	Hf (ppm)	176Lu/177Hf	176Hf/177Hf	±2σ	176Hf/177Hfi	εHf(t)	t (Ma)
YNG12-01	0.274	5.345	0.0073	0.282680	4	0.282677	-2.85	218
YNG12-03	0.281	5.040	0.0079	0.282665	3	0.282662	-3.39	218
YNG12-05	0.290	6.138	0.0067	0.282650	3	0.282647	-3.92	218
YNG12-08	0.303	6.661	0.0065	0.282669	6	0.282666	-3.24	218
QMX12-11	0.254	5.900	0.0061	0.282630	2	0.282628	-4.59	220
QMX12-01	0.363	6.252	0.0082	0.282663	2	0.282659	-3.48	220
QMX12-08	0.270	3.552	0.0108	0.282676	4	0.282671	-3.06	220
YDE12-02	0.525	3.702	0.0201	0.282675	4	0.282666	-3.24	228
RSX12-48	0.497	6.042	0.0117	0.282654	3	0.282649	-3.83	228
DL09-01	0.720	12.300	0.0083	0.282702	2	0.282698	-2.12	213*
DL09-03	0.670	10.900	0.0087	0.282689	2	0.282685	-2.59	213*

176Hf/177Hfi=[(176Hf/177Hf)-(176Lu/177Hf)(eλt-1)];

εHf(t)=[(176Hf/177Hfi)/(176Hf/177HfCHURi)-1]×104.

176Lu/177HfCHUR=0.0332; 176Hf/177HfCHUR=0.282772; λ(176Lu)=1.865×10-11yr-1.

*Age data come from Ding et al. (2011).

Table 6

Whole rock Pb isotopic composition of the late Triassic mafic dikes from the East Kunlun Orogenic Belt.

Sample	U (ppm)	Th (ppm)	Pb (ppm)	208Pb/204Pb	±2σ	207Pb/204Pb	±2σ	206Pb/204Pb	±2σ	208Pb/204Pbi	207Pb/204Pbi	206Pb/204Pbi	t (Ma)
YNG12-01	1.510	4.796	10.766	38.801	24	15.646	11	18.825	12	67.215	15.631	18.825	218
YNG12-03	1.017	4.164	11.254	38.803	27	15.651	13	18.801	14	62.403	15.641	18.801	218
YNG12-05	1.428	5.952	16.858	38.777	18	15.644	6	18.789	7	61.297	15.635	18.789	218
YNG12-08	2.448	5.810	12.620	38.841	50	15.648	17	18.850	9	68.205	15.627	18.850	218

208Pb/204Pbi=[(208Pb/204Pb)-(232Th/204Pb)(eλt-1)];

207Pb/204Pbi=[(207Pb/204Pb)-(235U/204Pb)(eλt-1)];

206Pb/204Pbi=[(206Pb/204Pb)-(238U/204Pb)(eλt-1)].

λ(232Th)=4.95×10-11yr-1; λ(235U)=9.85×10-10yr-1; λ(238U)=1.55×10-10yr-1.

Highlights

1. The (sub-) volcanic rocks from the East Kunlun Orogenic Belt formed at late Triassic.
2. Mafic dikes are derived from the metasomatized subcontinental lithospheric mantle.
3. Felsic volcanic rocks evolved from melts of juvenile crustal materials.
4. The (sub-) volcanic rocks are associated with post-collisional extension.